Published in: *Metal-Ceramic Interfaces* (eds. M. Rühle, A. G. Evans, M. F. Ashby and J. P. Hirth), Acta-Scripta Metallurgica Proceedings Series, Volume 4, Pergamon Press, 1990, pp 269-294.

MECHANICS AND THERMODYNAMICS OF BRITTLE INTERFACIAL FAILURE IN BIMATERIAL SYSTEMS

James R. Rice, Zhigang Suo and Jian-Sheng Wang
Division of Applied Sciences
Harvard University, Cambridge, MA 02138 USA

1. Introduction

We discuss elastic-brittle fracture theory for cracks along interfaces between elastically dissimilar solids. Crack tip fields in such cases are characterized by one real and one complex stress intensity factor, where the latter couples two of the classically separate crack tip modes. Solutions for complex stress intensity factors for a variety of cases, including geometries of interest for toughness testing, are cataloged and the theory is applied to the problem of dislocation nucleation from a crack tip along a dissimilar material interface, such as a metal/ceramic interface. The variation of the local phase angle, indicating stress field mode coupling, at the near atomic scale of dislocation nucleation is an important aspect of the problem. The dislocation problem arises in evaluating the competition between atomically brittle decohesion and plastic blunting at interfacial crack tips. Results confirm that both the properties of the interface and the direction of attempted cracking along it are important to the outcome of that competition; the latter arises because of the different stressing of slip systems associated with different directions of cracking. We also briefly review effects of solute adsorption at ceramic and metal/ceramic interfaces on their embrittlement, or in some cases on their ductilizing. Finally, we outline the thermodynamic interrelations between adsorption and alterations of the ideal work of interfacial separation, and formulate the thermodynamic theory in a manner consistent with the possibility of strong dissimilarity in adsorption properties of the two surfaces which joined at the interface before fracture.

2 Elastic Fields for Interface Cracks

In this section we briefly outline the form of near-tip fields from linear elastic continuum solutions for cracks along an interface between dissimilar materials. Such cracks are most simply modeled as surfaces across which no tractions are transmitted. Solutions resulting for that model generally predict material interpenetration very near the tip. However, that feature can often be ignored in interpreting the solutions, either because the predicted contact zone is small compared to physical sizes of interest like atomic spacings (as is the case in later applications here to dislocation nucleation at a crack tip) or larger scale measures of material heterogeneity, or because the predicted contact region occurs well within a near tip region in which mechanical loading may be characterized in terms of the singular fields of such elastic solutions (Rice, 1988). The case of joined isotropic materials, most discussed here, was analyzed between 1959 and 1965 by Williams, Cherepanov, England, Erdogan, Rice and Sih, and Malyshev and

Salganik; it has been the subject of much recent work (for references see Rice, 1988, Hutchinson, 1989, and Suo, 1989a). The case of cracks between dissimilar anisotropic solids was first analyzed by Gotoh in 1967 and by Clements and Willis in 1971 and has been discussed recently by Anderson (1988), Bassani and Qu (1989), Suo (1989a,c) and Wu (1989). A list of stress intensity factors and available specimens will be presented at the end of this section, which is intended to serve as a self-contained mini-reference for practitioners of the interface fracture mechanics.

2.1 Near tip stress fields. Ignoring terms which remain bounded at the tip, the near-tip stress field for an interface crack between dissimilar isotropic materials has the singular form (Fig. 1)

$$\sigma_{\alpha\beta} = \frac{1}{\sqrt{2\pi\, r}} \left[Re\, (K\, r^{i\varepsilon})\, \Sigma^{I}_{\alpha\beta}(\theta) + Im\, (K\, r^{i\varepsilon})\, \Sigma^{II}_{\alpha\beta}(\theta) + K_{III}\, \Sigma^{III}_{\alpha\beta}(\theta) \right] \quad (\alpha, \beta = x, y, z) \quad (2.1)$$

Here the angular functions $\Sigma_{\alpha\beta}(\theta)$ of superscripts I, II and III correspond to tractions across the interface at $\theta = 0$ of tensile, in-plane shear and anti-plane shear type, respectively, so that

$$(\sigma_{yy} + i\, \sigma_{yx})_{\theta=0} = \frac{K\, r^{i\varepsilon}}{\sqrt{2\pi\, r}}, \qquad (\sigma_{yz})_{\theta=0} = \frac{K_{III}}{\sqrt{2\pi\, r}}, \quad (2.2)$$

and in this sense those $\Sigma_{\alpha\beta}(\theta)$ may be said to correspond to modes I, II and III. However $\Sigma^{I}_{\alpha\beta}(\theta)$ and $\Sigma^{II}_{\alpha\beta}(\theta)$ also depend on elastic properties of the bimaterial combination, through the parameter ε to be discussed, and do not have the full symmetry and anti-symmetry respectively associated with such angular functions for the case of a crack tip in a homogeneous solid. The functions are given in the Appendix and plotted in Fig.2. The parameter ε is given by

$$\varepsilon = \frac{1}{2\pi} ln \left[\frac{(3 - 4\nu_1)/\mu_1 + 1/\mu_2}{1/\mu_1 + (3 - 4\nu_2)/\mu_2} \right] \quad (2.3)$$

where μ is shear modulus and ν the Poisson ratio, and subscripts refer to the two materials (Fig. 1).

The K_{III} is a mode III stress intensity factor of familiar type, but rather than having mode I and II factors, there is a single complex stress intensity factor K for the in-plane modes, and these modes are inherently coupled together. This complex K has the generic form

$$K = Y\, T \sqrt{L}\, L^{-i\varepsilon}\, e^{i\psi} \quad (2.4)$$

(examples are given subsequently) where T is a representative magnitude of the stress applied to load the specimen, L a characteristic length (e. g., crack length, layer thickness), Y a dimensionless real positive quantity, and ψ by definition is the phase angle of $K\, L^{i\varepsilon}$, but is often loosely called the phase angle of the complex stress intensity factor, or the phase angle of the applied load. (A better characterization of the phase is given below.) Both Y and ψ are dependent on the detailed manner of applying the stress T and, in general, on the ratios of elastic moduli and of characteristic dimensions of the cracked body to one another.

Thus, considering eqs.(2.1,2), the analogs of K_I and K_{II} for the bimaterial case are not constants but are instead functions of r, that we might denote as $K_I(r)$ and $K_{II}(r)$, given by

$$K_I(r) \equiv Re\, (K\, r^{i\varepsilon}) = Y\, T \sqrt{L}\, cos\, [\psi - \varepsilon\, ln\, (L/r)] ,$$

$$K_{II}(r) \equiv Im\,(K\, r^{i\varepsilon}) = Y\, T \sqrt{L}\, sin\, [\psi - \varepsilon\, ln\, (L/r)]. \tag{2.5}$$

Evidently the ratio $\sigma_{yx}/\sigma_{yy} = K_{II}(r)/K_I(r) = tan\, [\psi - \varepsilon\, ln\, (L/r)]$ varies with r near the tip, so that the tensile and in-plane shear modes are fundamentally inseparable. The variable quantity $\psi - \varepsilon\, ln\, (L/r)$ gives what might be called the *local phase angle* of the field; a similar concept was introduced by Liechti and Hanson (1988).

To better characterize phase, we may choose some fixed length $\hat{r}$. It does not matter whether we choose $\hat{r}$ as 1 nm, or 1 mm, or 1 m, or whatever, so long as we regard it as held fixed when specimens of a given bimaterial combination corresponding to a range of values of L and ψ are considered. Then a suitable absolute characterization, say $\hat{\psi}$, of the phase angle is given by writing

$$K_I(\hat{r}) + i\ K_{II}(\hat{r}) \equiv K\, \hat{r}^{\,i\varepsilon} = \sqrt{\left[K_I(\hat{r})\right]^2 + \left[K_{II}(\hat{r})\right]^2}\ e^{i\hat{\psi}} = Y\, T \sqrt{L}\, (\hat{r}/L)^{i\varepsilon}\, e^{i\psi} \tag{2.6}$$

so that

$$\hat{\psi} = \psi - \varepsilon\, ln(L/\hat{r}). \tag{2.7}$$

In citing the value of $\hat{\psi}$ to be associated with a given specimen, clarity requires that one also report the value of $\hat{r}$. A set of $\hat{\psi}$ values based on the fixed length $\hat{r}_A$ differs from a set based on another fixed length, $\hat{r}_B$, by a constant angle, i. e., $\hat{\psi}_A - \hat{\psi}_B = \varepsilon\, ln(\hat{r}_A/\hat{r}_B)$, for every member of the set. If $\hat{r}$ is chosen as some length on the laboratory scale in crack studies, say $\hat{r}$ = 1 mm, then for typical small ε (see Table I) the difference between $\hat{\psi}$ and ψ will be small for all L in a fairly broad range, say 0.1 to 10 mm.

In the above discussion there is no fundamental meaning attached to the quantities denoted by $K_I(\hat{r})$ and $K_{II}(\hat{r})$, since $\hat{r}$ is chosen arbitrarily. Nevertheless, because of the weak $ln(L/r)$ variation with r in eqs.(2.5), and because ε is typically very small, the trigometric functions of (2.5) are often little changed by fractionally large changes in r. E. g., for $\varepsilon = 0.05$, which is fairly large, a factor of 5 change in r alters the arguments of the trigometric functions by $\varepsilon\, ln\, 5 \equiv 0.08 \equiv 5^o$. Because of that, it can sometimes be justified to evaluate $K_I(r)$ and $K_{II}(r)$ at a fixed material distance $\hat{r}$, thought to be broadly representative of the size of the "fracture process zone" for a given bimaterial, and then to consider $K_I(\hat{r})$ and $K_{II}(\hat{r})$ as classical mode I and II intensity factors. Our subsequent treatment of dislocation nucleation at an interfacial crack tip can be interpreted in that way, based on an atomic sized $\hat{r}$. Of course, K rigorously reduces to the classical $K_I + i\, K_{II}$ only when $\varepsilon = 0$, i. e., when β as defined below is zero.

Joined anisotropic solids. The singular stress field near the tip of an interface crack between dissimilar anisotropic solids can also be put in the form of eq.(2.1), in the sense that the field can be characterized by one real stress intensity factor and one complex factor, the latter multiplying a term $r^{i\varepsilon}$ (e. g., Suo, 1989a,c, Wu, 1989), except that now the analogs of the angular functions Σ^I, Σ^{II}, and Σ^{III} of (2.1) no longer correspond, in general, to respective tractions of tensile, in-plane shear, and anti-plane shear type along the interface ahead of the tip.

When the material symmetries of joined anisotropic solids are such that in-plane loadings produce no

anti-plane deformations, and conversely, the real intensity factor K_{III} still corresponds to stresses of type σ_{yz} on the interface (i. e., to conventional mode III), as remarked by Bassani and Qu (1989). However, cases exist for which the real intensity corresponds to stress of type σ_{yy} ("mode I") on the interface, and for which σ_{yx} ("mode II") and σ_{yz} ("mode III") there are characterized by a complex K with $\varepsilon \neq 0$, and hence are coupled and oscillatory when that $K \neq 0$. This situation occurs, in general, for interface cracks in symmetric tilt bicrystals (i. e., two crystals of the same material in mirror-image orientation relative to one another). By symmetry, the loading of such bicrystals solely by symmetric tensile forces relative to the interface produces only σ_{yy} and no σ_{yx} or σ_{yz} on the interface; hence such loadings produce complex $K = 0$ in that case and generate only a classical, non-oscillatory mode I singularity characterized by a real intensity factor. When the crack tip coincides with the tilt axis of such a symmetric tilt bicrystal, and when that common axis is also an axis of crystal symmetry such that in-plane and anti-plane deformations decouple (e. g., [100], [110], or [111] axes in cubic crystals), it turns out, as could be anticipated from the special cases discussed so far, that $\varepsilon = 0$ and the entire crack tip stress state is then non-oscillatory under general loading (Bassani and Qu, 1989).

Ting (1986) has given the general formula for calculating ε in terms of the anisotropic modulus tensors of the two joined solids and also proven a remarkable theorem which shows that for a given pair of orientations of two dissimilar anisotropic crystals, ε is invariant to rotations of the interface plane about the crack tip. Since $\varepsilon = 0$ in the special cases involving symmetric tilt bicrystals noted in the last sentence of the previous paragraph, it then follows from the Ting theorem that $\varepsilon = 0$ also for interface cracks in bicrystals that are asymmetrically tilted about an axis of crystal symmetry for which in-plane and anti-plane deformations decouple, so long as the crack tip is along that tilt axis. In cases of interfacial cracks between anisotropic solids with $\varepsilon = 0$, it need not follow in general that the complex K reduces to the classical $K_I + i K_{II}$ (Suo, 1989a.c).

2.2 Values of ε for joined isotropic solids. As observed by Dundurs (1969), for a bimaterial composite of isotropic constituents under plane strain conditions, with traction prescribed on the boundary, stresses in the body depend on only *two* dimensionless moduli combinations, α and β, defined as

$$\alpha = \frac{(1-\nu_2)/\mu_2 - (1-\nu_1)/\mu_1}{(1-\nu_2)/\mu_2 + (1-\nu_1)/\mu_1}, \quad \beta = \frac{1}{2}\frac{(1-2\nu_2)/\mu_2 - (1-2\nu_1)/\mu_1}{(1-\nu_2)/\mu_2 + (1-\nu_1)/\mu_1} \quad \left[\varepsilon = \frac{1}{2\pi} ln\left(\frac{1-\beta}{1+\beta}\right)\right]; \qquad (2.8)$$

α measures the relative stiffness of the two materials. By requiring $0 < \nu < 1/2$ and $\mu > 0$, Dundurs showed that α and β are confined to a parallelogram in the (α, β) plane with vertices at (1, 0), (1, 0.5), (-1, 0) and (-1, -0.5), so that the maximum possible $|\varepsilon| = 0.175$. Calculations by Suga et al. (1988) on more than a hundred material pairs suggest that the values of β are even more restricted, i.e., $|\beta| < .25$, implying that $|\varepsilon| < 0.08$. Representative values of these parameters are given in Table I. The elastic constants used for the calculations are taken from Hirth and Lothe (1982) for all single elements and Suga et. al (1988) for sapphire (Al_2O_3) fiber and MgO. Note that α, β and ε reverse sign when materials 1 and 2 are interchanged.

TABLE I Dundurs parameters and the oscillatory index ε.

bimaterial (mat'l 1 / mat'l 2)	α	β	ε
Al /Sapphire	–.69	–.143	.046
Au /Sapphire	–.62	–.053	.017
Cu /Sapphire	–.47	–.096	.031
Nb /Sapphire	–.55	–.056	.018
Ni /Sapphire	–.26	–.063	.020
Fe /Sapphire	–.30	–.065	.021
Au /MgO	–.53	–.062	.020
Ni /MgO	–.13	–.079	.025
Cu /Si	–.04	.038	–.012

2.3 Catalog of solutions for complex K. *i) An internal crack*: Analyses of collinear interface cracks between two half-planes of dissimilar materials were the subject of 1965 papers by England, Erdogan, and Rice and Sih. As an example, for an internal crack of length 2a with stress state $(\sigma^{\infty}_{yy}, \sigma^{\infty}_{yx})$ at infinity (Fig. 3), the stress intensity factor at the *right-hand* crack tip is

$$\begin{aligned} K &= (1 + 2i\,\varepsilon)\left(\sigma^{\infty}_{yy} + i\,\sigma^{\infty}_{yx}\right)\sqrt{\pi a}\,(2a)^{-i\varepsilon} \\ &= T\,e^{i\,[\,\omega + \arctan(2\varepsilon)\,]}\,\sqrt{(1+4\varepsilon^2)\,\pi a}\,(2a)^{-i\varepsilon} \end{aligned} \tag{2.9}$$

We have used $\sigma^{\infty}_{yy} + i\,\sigma^{\infty}_{yx} = T\,e^{i\omega}$ in the latter form, where T is the magnitude of the remotely applied traction vector and ω is its angle with the y direction, to give agreement with the form of eq.(2.4). Thus the phase angle ψ in this case is $\omega + \arctan(2\varepsilon) \cong \omega$. Notice that the material dependence of K in (2.7) is through ε only. This is a feature common to all problems of collinear interface cracks between two half planes under self-equilibrated traction on crack faces.

ii) Crack/dislocation interactions: The problems of cracks interacting with various singularities (dislocation, line force, transformation spot, etc.) are solved in Suo (1989a,b). The stress intensity factor, for instance, of a semi-infinite crack due to a dislocation with Burgers vector $b = b_y + i\,b_x$ at point $s = x_0 + i\,y_0$ in material 2 (Fig. 4) is

$$K = -\frac{E^*\cosh\pi\varepsilon}{4\sqrt{2\pi}}\left[\left(e^{-\pi\varepsilon}\,\bar{s}^{\,-1/2-i\varepsilon} + e^{\pi\varepsilon}\,s^{-1/2-i\varepsilon}\right)b + (1/2 + i\varepsilon)\,e^{\pi\varepsilon}\,(s-\bar{s})\,s^{-3/2-i\varepsilon}\,\bar{b}\right] \tag{2.10}$$

where 1/E* is the average of $(1-\nu)/2\mu$ for the two materials. One must change πε to -πε everywhere to obtain K when the dislocation is in material 1.

iii) A thin film under residual tension: Consider a thin film of thickness h, deposited on an elastic substrate, with residual tensile stress σ in the film (Fig. 5a). The induced stress intensity factor for a long crack is given by

$$K = \sqrt{\frac{1-\alpha}{2\left(1-\beta^2\right)}}\;\sigma\,h^{1/2-i\varepsilon}\;e^{i\psi(\alpha,\beta)} \tag{2.11}$$

where α and β are the Dundurs' parameters. The phase angle $\psi(\alpha, \beta)$ is plotted in Fig. 5b for $\beta = 0$ (the error due to $\beta \neq 0$ is small). This problem was solved in Suo and Hutchinson (1989a). The thickness of the substrate is assumed to be infinite in (2.11). Solutions for finite substrates can be found in the original paper. Argon et al. (1989) have used residual stresses in thin films as driving forces to measure interface toughness.

iv) Sandwich specimens: Any homogeneous specimen can be converted to measure interface toughness by sandwiching a *thin* second material layer of thickness h, Fig.6a. The residual stress in the thin layer does not contribute to K and, in calibrating such a specimen, one needs to take account of the external loading only. This arrangement has been experimentally tested by Oh et al. (1987) and Cao and Evans (1989) with various reference homogeneous specimens. The measured critical loads are first used to calculate the classical stress intensity factors K_I and K_{II} as if the specimen were homogeneous (i. e., as if h = 0) using, for instance, the standard handbook solutions. The latter are then converted to the interface stress intensity factor K. A universal conversion relation, which is independent of the geometry of the reference homogeneous specimen when h is small, is (Suo and Hutchinson, 1989b)

$$K = \sqrt{\frac{1-\alpha}{1-\beta^2}}\left(K_I + i\ K_{II}\right) h^{-i\varepsilon}\, e^{i\,\omega(\alpha,\,\beta)} \tag{2.12}$$

The phase angle shift relative to the classical stress intensity factor, $\omega(\alpha, \beta)$, is typically small and is plotted in Fig. 6b with $\beta = 0$.

v) A bending specimen: The specimen illustrated in Fig.7a was analyzed by Charalambides et al. (1989a,b) and Suo and Hutchinson (1989a). When the crack is long compared with the thickness of the notched layer, h, the stress intensity factor is of the form

$$K = Y(\alpha,\, \beta,\, h/H)\, M\, h^{-3/2-i\varepsilon}\, e^{i\,\psi\,(\alpha,\,\beta,\,h/H)} \tag{2.13}$$

where M is the moment per unit width, and Y and ψ as the functions of α and h/H are plotted in Figs. 7b and 7c, with $\beta = 0$. Thermal mismatch stress between the two layers is a driving force for crack extension and analysis of that can be found in the above cited papers.

2.4 Crack opening displacement and energy release rate. Letting δ_α denote components of the relative displacement of two initially coincident points along the crack walls, for isotropic solids

$$\delta_y + i\ \delta_x = \left(\frac{1-\nu_1}{\mu_1} + \frac{1-\nu_2}{\mu_2}\right)\frac{K\, r^{i\varepsilon}\sqrt{2\,r}}{\sqrt{\pi}\,\cosh(\pi\varepsilon)\,(1+2i\,\varepsilon)}\,, \qquad \delta_z = \left(\frac{1}{\mu_1} + \frac{1}{\mu_2}\right)\frac{K_{III}\sqrt{2\,r}}{\sqrt{\pi}} \tag{2.14}$$

very near the tip, and the Irwin-type energy release rate expression is

$$G = \left(\frac{1-\nu_1}{\mu_1} + \frac{1-\nu_2}{\mu_2}\right)\frac{K\,\overline{K}}{4\cosh^2(\pi\varepsilon)} + \left(\frac{1}{\mu_1} + \frac{1}{\mu_2}\right)\frac{K_{III}^2}{4} \tag{2.15}$$

where we note that $K\,\overline{K} = Kr^{i\,\varepsilon}\,\overline{Kr^{i\,\varepsilon}} = [K_I(r)]^2 + [K_{II}(r)]^2 = Y^2\,T^2\,L$ in the notation of eq.(2.4).

2.5 Contact and range of validity of complex K. Since eqs.(2.5) show that $Kr^{i\varepsilon}$ oscillates with r as $r \to 0$, (2.14) shows that the condition $\delta_y < 0$ (i. e., predicted interpenetration) must occur for some

sufficiently small r. We can estimate the distance r_{con} over which contact occurs near the tip as approximately twice the r at which δ_y or σ_{yy} is first predicted to turn negative by the solutions that ignore contact (more precise analyses of the near tip contact problem, within linear elastic theory, have been given by Comninou, 1977, and Comninou and Schmueser, 1979). Thus for small $\varepsilon > 0$

$$r_{con} \cong 2L\, exp[-(\psi + \pi/2)/\varepsilon] \ , \tag{2.16}$$

and one just changes ε to $-\varepsilon$, and ψ to $-\psi$ in this equation when $\varepsilon < 0$.

The predicted r_{con} is sometimes of subatomic size. For example, taking L = 5mm, we may ask how small ε must be for the predicted r_{con} to be less than an atom spacing ($\cong$0.25 nm). Considering material combinations with $\varepsilon > 0$, the condition is met whenever $\varepsilon < 0.069$ if $\psi = +45^o$, whenever $\varepsilon < 0.046$ if $\psi = 0^o$, and whenever $\varepsilon < 0.023$ if $\psi = -45^o$. These conditions are met by most of the combinations in Table I, and by all if we consider only angles $\psi > 0$. When $\varepsilon > 0$, r_{con} becomes negligible (subatomic, for any laboratory sized L) as $\psi \to 90^o$, but r_{con} becomes of order L as $\psi \to -90^o$. The converse holds for combinations with $\varepsilon < 0$.

The predicted near tip contact, of which the scale is not always subatomic as above, has generally been regarded as an obstacle to the development of interface fracture mechanics. Clearly, the forms given here for the near tip stress and displacement fields must be wrong on some sufficiently small scale. However, as Rice (1988) has recently emphasized in discussing the plane strain state, the parameter K entering those fields does nevertheless characterize the severity of the near-tip loading whenever the size of a zone involving any or all of interface contact, nonlinear material response (plasticity, smaller scale microcracking, transformation), or dominance by discreteness of material microstructure (atom spacing in a crystal, fiber spacing in a composite treated globally as a continuum, etc.) is much smaller than characteristic macroscale dimensions like crack length. Thus just as K_I, K_{II} and K_{III}, and their histories, uniquely characterize the near tip state in conventional fracture mechanics, whenever such a size restriction is met, so also do (complex) K and K_{III} in interface fracture mechanics. In fact, the singular stress and displacement fields discussed here provide an intermediate asymptotic description of those fields over a range of r much smaller than a characteristic length like L but much larger than the near tip zone dominated by contact, nonlinearity and/or discreteness; the K concept is valid when such an intermediate length scale exists.

2.6 Fracture toughness for interface cracks. Consider a bimaterial specimen with a pre-existing interface crack and assume for simplicity that it is loaded so as to induce only in-plane stresses of type σ_{yy} and σ_{yx} (but no mode III stress σ_{yz}) on the interface ahead of the tip. Since tension and shear are inherently coupled for the interface crack, there can be no unambiguous characterization of a mode I and mode II toughness. Instead the toughness must be represented as a magnitude $|K|$ ($= \sqrt{K\,\overline{K}} = Y\,T\,\sqrt{L}$) of K for each value of the phase angle of interest, and the phase angle is properly reported as $\hat{\psi}$ of (2.6) based on a chosen (and specified) $\hat{r}$. One loads the specimen proportionally (thus ψ and $\hat{\psi}$ are fixed), records the magnitude of the loading stress, T, at the onset of crack propagation, and then, with a relation of form (2.4) appropriate for the specimen, calculates the corresponding $|K|$. Repeating this procedure

systematically for various $\hat{\psi}$, e.g., by changing the relative proportions of various loads, or by changing crack length or specimen design, one obtains a $|K|_c$-$\hat{\psi}$ curve, referred to as the *toughness locus* of the interface, where the subscript c denotes the critical value. Within the framework of elastic fracture mechanics, this curve is a property of the interface, which is independent of the specimen geometry and loading system. Since |K| is related to the energy release rate G by (2.15), it is equivalent to report a G_c-$\hat{\psi}$ curve instead.

Clearly, the oscillating singularity of the interface crack problem does not present any essential difficulty in engineering application of the macroscopic fracture mechanics methodology. Rather, it is the *mode mixity* that complicates the method. A crack in an isotropic, homogeneous brittle solid can usually adjust itself onto a path with the mode I state at the tip. For this reason, classical fracture mechanics requires information primarily about only one material property, namely, K_{Ic}. By contrast, since an interface is often an easy fracture path, compared to one through the adjoining bulk materials, a crack, even if subjected to substantial shear stresses ahead the tip, may tend to stay along the interface. Consequently, instead of one material property, one needs a *curve*, or toughness locus, to fully characterize the toughness of an interface.

Experimental determination of interface toughness has been attempted recently on several model systems (Argon et al., 1989, Cao and Evans, 1989, Charalambides et al., 1989a,b, Oh et al., 1987), with only one of them (Cao and Evans) covering a relatively wide range of mode mixity. In principle, any geometry with an interfacial crack, with a calibration relation in the form of (2.4) connecting measurable driving forces and stress intensity factors, may be used as a specimen for measuring interface toughness. Thin films under residual tension, sandwiches, and bending specimens, all discussed in section 2.3, seem to be especially suitable for measuring toughness of brittle interfaces.

3. Crack Tip Competition: Interface Cleavage versus Dislocation Emission

The Kelly-Tyson-Cottrell (Kelly et al, 1967) and Rice-Thomson approaches (Rice and Thomson, 1974) have focussed on the competition of dislocation emission and atomic decohesion at a crack tip as a test of whether a given ductile crystal is intrinsically cleavable. The R-T approach has also been extended to interfaces between ductile crystals (Rice, 1976; Mason, 1979; Anderson and Rice, 1986; Rice, 1987; Anderson et al., 1989; Wang and Anderson, 1989) but, so far, no account has been included of effects like those discussed in the last section of dissimilarity of elastic properties across such an interface. We do so here in the form of a simple version of the R-T model, and apply it to certain orientations of ductile fcc metal crystals that are joined to brittle ceramics.

In recent evaluations of the R-T model starting with Mason (1979), the energy release rate calculated as necessary for dislocation emission from a crack tip, G_{disl}, is compared to that for cleavage, G_{cleav}, where the latter is understood as atomistically brittle decohesion of the interface. If $G_{cleav} > G_{disl}$, one expects that a dislocation will emanate from the crack tip, producing a blunted crack and spoiling the stress concentration, before conditions for atomic decohesion can occur. It is then assumed that failure, if to

occur from processes at that crack tip, must be by some ductile mechanism, at least when there is adequate mobility of dislocations in moving away from the crack tip once they have been generated there. Conversely, if $G_{disl} > G_{cleav}$, the crack tip remains stable against dislocation blunting, i. e., atomically sharp, and it is assumed that atomic decohesion can occur leading to a cleavage-like brittle interfacial fracture. We then say that the interface is intrinsically cleavable from that crack tip. The qualifyer "intrinsically" emphasizes that in materials capable of plastic flow the matter of whether cleavage will actually occur is strongly dependent on plastic flow properties (and hence on hardness, loading rate and temperature). This is because the ease of plastic flow in material surrounding the crack tip which will control whether that tip remains atomically sharp against externally generated dislocations that may move towards it along slip planes, and also whether the surroundings can support enough stress to actually allow the condition $G = G_{cleav}$ to be attained locally at such an atomically sharp crack. Metal/ceramic interfaces that are judged not to be intrinsically cleavable may, of course, sometimes fail by atomically brittle cracking near the interface in the ceramic.

Aspects of interfacial fracture other than those reflecting dissimilarity of properties of the two adjoining materials, which is the focus here, have been reviewed recently by Rice and Wang (1989) and the reader is referred there for further discussion.

3.1 Cleavage decohesion. The simplest model of cleavage decohesion is provided by the elastic-brittle Griffith model, which estimates G_{cleav} as the work $2\gamma_{int}$ of reversibly separating unit area of interface:

$$G_{cleav} = 2\gamma_{int} \tag{3.1}$$

where, in absence of matter diffusion to or from the interface during separation (see section 4),

$$2\gamma_{int} = f_{s,1} + f_{s,2} - f_{1/2} \tag{3.2}$$

Here subscripts 1 and 2 refer to the two solids, $f_{s,1}$ and $f_{s,2}$ are surface free energies for the faces of solids 1 and 2 that are exposed by fracture and $f_{1/2}$ is the free energy of the 1/2 interface existing before fracture.

Cohesive zone models incorporate some further details of the separation process. In the simplest versions, containing no account of lattice discreteness in directions parallel to the interface, the interfacial region is represented as two joined elastic continua which interact with one another such that a stress versus separation relation, $\sigma_{y\alpha} = \partial\phi(\delta_x, \delta_y, \delta_z)/\partial\delta_\alpha$ ($\alpha = x, y, z$) applies along the gradually decohering interface. Here ϕ is the potential of the cohesion, $\phi(0, 0, 0)$ corresponds to $f_{1/2}$, and $\phi(\delta_x, \infty, \delta_z)$ to $f_{s,1} + f_{s,2}$. Provided that the two crack walls can be pulled apart quasistatically to full separation, in a crack-like mode, without local dynamic instabilities or dislocation or other inelastic processes within the two solids, a well known argument based on the J integral shows that this model gives the same result as (3.1,2), at least in typical circumstances when the zone undergoing decohesion is much shorter than the overall crack length (e. g., Rice, 1987).

However, effects relating to lattice discreteness cause local instabilities during separation and make $2\gamma_{int}$ a lower bound to G_{cleav} even when no dislocations are left in the material after passage of the crack.

One such effect is "lattice trapping"; current estimates (e. g., Thomson, 1983, 1986) suggest that it only slightly raises G_{cleav} above $2\gamma_{int}$. Another effect, which has not yet been quantified but may be important given the inevitably coupled x and y direction displacing that will occur during interfacial separation between materials of strong dissimilarity in elastic properties (in which effects relating to the presence of ε of the last section are non-negligible), involves local instabilities in shear displacement effectively corresponding to dislocation formation in the interface region as it is being pulled apart.

3.2 Dislocation emission. Conditions for dislocation emission on a particular slip system are not fundamentally expressible as a critical value of G, but rather as some critical value of a linear combination of K_I, K_{II}, and K_{III} (or their generalizations like in eqs.2.5) which characterize the shear stress along that slip plane. Thus while G_{cleav} may be regarded as constant, at least within the Griffith model, G_{disl} will not have a fixed value but, rather, will depend on the ratios of the K's to one another.

For example, the shear stresses on a slip plane which intersects the interface along the crack tip (fig. 8) are $\sigma_{\theta r}$ and $\sigma_{\theta z}$. Resolving these in the direction of the Burgers vector **b** for that system, with edge and screw components b_r and b_z, respectively, gives the force driving a straight dislocation line away from the crack tip as

$$f_{emit} = \sigma_{\theta r} b_r + \sigma_{\theta z} b_z = \frac{b}{r^{1/2}} \left[Re\,(K\, r^{i\varepsilon})\, S_I + Im\,(K\, r^{i\varepsilon})\, S_{II} + K_{III}\, S_{III} \right] \qquad (3.3)$$

where b is the magnitude of **b**, the dislocation line is at distance r from the tip, the $\sigma_{\alpha\beta}$ ($\alpha, \beta = r, \theta, z$) are the stresses of (2.1), and each S_J is defined by

$$S_J = [(b_r/b)\, \Sigma^J_{\theta r}(\theta) + (b_z/b)\, \Sigma^J_{\theta z}(\theta)] / \sqrt{2\pi} \qquad (J = I, II, III)\ . \qquad (3.4)$$

Here θ is the angle of the slip plane (fig. 8) and the $\Sigma_{\alpha\beta}$ are from (2.1). For joined isotropic solids

$$S_I = \Sigma^I_{r\theta}(\theta)\, cos\ \phi / \sqrt{2\pi}\ ,\ \ S_{II} = \Sigma^{II}_{r\theta}(\theta)\, cos\ \phi / \sqrt{2\pi}\ ,\ \ S_{III} = cos\ \theta/2\, sin\ \phi / \sqrt{2\pi} \qquad (3.5)$$

where $\Sigma^I_{r\theta}(\theta)$ and $\Sigma^{II}_{r\theta}(\theta)$ are given in the Appendix and plotted in fig. 2, and ϕ is the angle which the Burgers vector makes with the normal to the crack tip, fig.8. Eqs.(3.3,4) are also valid for joined anisotropic solids with the interpretations given earlier.

The "image" force component opposing outward motion of the dislocation line, and drawing it back into the tip, has been solved for by Rice (1985) for the general case of joined anisotropic solids. Remarkably, it depends only on the elastic properties of the material (1, in the present case) in which the dislocation resides, and is

$$f_{image} = \frac{1}{r} b_\alpha A_{\alpha\beta} b_\beta \qquad (3.6)$$

where $A_{\alpha\beta}$ is the pre-logarithmic energy factor matrix of a straight dislocation line in that material, i. e., $b_\alpha A_{\alpha\beta} b_\beta$ is the factor which appears when the energy per unit length of dislocation line is written as $E_{dislocation} = b_\alpha A_{\alpha\beta} b_\beta\, ln\,(r_{outer}/r_{core})$. When material 1 is isotropic

$$A_{rr} = A_{\theta\theta} = \frac{\mu_1}{4\pi\,(1-\nu_1)}\ ,\ \ A_{zz} = \frac{\mu_1}{4\pi}\ ,\ \text{other } A_{\alpha\beta} = 0\ . \qquad (3.7)$$

Thus, using the simplified emission criterion (e. g., Thomson, 1986) that $f_{emit} = f_{image}$ for $r = r_c$, the dislocation core size, which also assures that $f_{emit} > f_{image}$ for all $r > r_c$, the critical combination of intensity factors estimated as necessary for dislocation emission is given by

$$\left(Re\,(K\, b^{i\varepsilon})\, S_I + Im\,(K\, b^{i\varepsilon})\, S_{II} + K_{III}\, S_{III} \right)_{disl} = b_\alpha A_{\alpha\beta} b_\beta / [\, b\, r_c^{1/2}\,]$$
$$\left(= \mu_1\, b\, [cos^2\phi + (1-\nu_1)\, sin^2\phi\,] / [\, 4\pi\,(1-\nu_1)\, r_c^{1/2}\,] \text{ for isotropic solid 1} \right) \qquad (3.8)$$

Here we have taken advantage of the fact that $K\, r^{i\varepsilon}$ is a slowly varying function of r, given the small values of ε, in the sense that $K\, r^{i\varepsilon} \cong K\, b^{i\varepsilon}$ for all r of order b and, since core size r_c will always be of order b, we have just replaced $K\, r^{i\varepsilon}$ by $K\, b^{i\varepsilon}$ in (3.3).

Atomic scale phase angle ψ'. We may write

$$K\, b^{i\varepsilon} = |K|\, e^{i\psi'} = cosh\ \pi\varepsilon\ \sqrt{G\, E^*}\ \ e^{i\psi'} \qquad (3.9)$$

where, again, $1/E^*$ is the average of $(1-\nu)/2\mu$, so that this equation defines an *atomic scale phase angle*, denoted as ψ'. It is related to the angle ψ in the generic form of (2.4) for K by

$$\psi' = \psi - \varepsilon\, ln\ (L/b)\,. \qquad (3.10)$$

This ψ' is just a special version of $\hat{\psi}$ of eq.(2.7) but, unlike the typical situation for $\hat{\psi}$ when the $\hat{r}$ on which it is based is chosen to be on the laboratory scale, the difference between ψ' and ψ will typically be significant. This is because L is generally macroscopic and b is of order 0.25 nm. For example, if $L \cong 5$ mm, $\psi' \cong \psi - 17\,\varepsilon$, which is a significant change from ψ even for the smaller ε in Table I. As a consistency check, one should assure that $-\pi/2 < \psi' < +\pi/2$ for use of the above expressions for dislocation nucleation; the condition effectively assures that interpenetration is not predicted over a scale as large as a lattice spacing near the crack tip.

Finally, considering joined isotropic solids under in-plane loadings, so that $K_{III} = 0$ and the near tip field is fully characterized by K, G_{disl} may be calculated from (3.8) and (2.15). After using (2.8) to rearrange some terms, the result is

$$G_{disl} = \frac{\mu_1\, b^2}{(1-\nu_1)\,(1-\alpha)\, r_c} \left[\frac{cos\ \phi + (1-\nu_1)\, sin\ \phi\ tan\ \phi}{4\sqrt{\pi}\ cosh\ \pi\varepsilon \left(\Sigma^{I}_{r\theta}(\theta)\, cos\ \psi' + \Sigma^{II}_{r\theta}(\theta)\, sin\ \psi' \right)} \right]^2 \qquad (3.11)$$

It is seen that G_{disl} depends on the phase angle ψ', and hence on the mode mixity of the applied loadings. In fact, the above result applies only for the range of ψ' such that $\Sigma^{I}_{r\theta}(\theta)\, cos\ \psi' + \Sigma^{II}_{r\theta}(\theta)\, sin\ \psi' > 0$; otherwise, the direction of shearing along the slip plane considered does not tend to drive a dislocation away from the tip, and emission cannot occur on that plane. Since G_{cleav} is independent of ψ', at least for the Griffith model, it may occur that $G_{disl} < G_{cleav}$ for one range of ψ' and $G_{disl} > G_{cleav}$ for another. Thus the nature of crack tip response is not universal but depends on the mode mixity of the applied loading.

Previous studies based on non-oscillatory crack tip fields and semi-circular loop model. We note that the modeling of dislocation emission from an interfacial crack tip is somewhat more advanced in cases for which there is a conventional non-oscillatory singularity at the tip. These cases are equivalent to setting ε

= 0 in the representations of the near-tip field here and letting K denote the classical $K_I + i K_{II}$. Such cases include symmetric tilt bicrystals as discussed earlier.

Here we summarize recent studies modeling the emission of a semi-circular dislocation loop from a crack tip (Anderson ,1986; Anderson and Rice, 1986; Wang et al., 1987; Wang and Anderson, 1989). These studies proceed like in Mason (1979), calculating the energy U of a semi-circular loop of radius R introduced into a stressed solid at the crack tip, and determine R, as well as the combination $K_I S_I + K_{II} S_{II} + K_{III} S_{III}$ (with the S_J defined as in eq. 3.4), at nucleation from the conditions that $\partial U/\partial R = 0$ and $\partial^2 U/\partial R^2 = 0$. The result is

$$(K_I S_I + K_{II} S_{II} + K_{III} S_{III})_{disl} = 0.76 \frac{A_o}{b} \sqrt{\frac{m}{r_c}}\ exp\ (E_{ledge}/\pi A_o) \qquad (3.12)$$

Here A_o is the pre-logarithmic energy factor appearing in the expression $U = 2\pi R A_o ln(8R/e^2 r_c)$ for the energy of a full circular shear loop of the same orientation in an uncracked solid; $A_o = (2-\nu)\mu b^2/8\pi(1-\nu) \cong \mu b^2/10$ for an isotropic solid. E_{ledge} is the energy of the ledge produced at the blunted crack front due to dislocation emission; Anderson (1986) estimates $E_{ledge}/\pi A_o \cong 0.1$ to 0.6 for various cubic metals. The factor m has been calculated for shear loops at a crack tip by Gao and Rice (1989); it arises in the exact (within continuum elasticity) expression $U = \pi R A_o ln(8mR/e^2 r_c)$ for the self energy of a semi-circular shear loop of radius R emanating from the crack tip; m depends on θ and ϕ (fig. 8) with typical values in the range from about 1 to 2.

For some materials dislocations may be nucleated in dissociated form as a pair of partials. In that case terms related to the stacking fault energy and the interaction energy between the partials must be included (Anderson, 1986; Anderson and Rice, 1986; Wang and Anderson, 1989). Taking m = 1.5, $E_{ledge}/\pi A_o$ = 0.3 and $\phi = 30^o$ as representative, and using expressions for identical isotropic solids with $\nu = 0.3$, predictions from the simpler model leading to (3.8) and the presumably more exact expression of (3.12) can be compared. The results are fairly close to one another; the former gives $0.11\mu b/r_c^{1/2}$ and the latter $0.13\mu b/r_c^{1/2}$ for the value of $K_I S_I + K_{II} S_{II} + K_{III} S_{III}$ at nucleation.

Bicrystal experiments. Although as noted earlier, the R-T model does not address important facets of ductile versus brittle failure relating to viscoplastic material response, the model has enabled rationalization of observed intrinsic behavior for various systems. These include the orientation and cracking direction dependence for a series of [110] symmetric tilt Cu-Bi alloy bicrystals, with interfacial cracks introduced in directions such that their tips are along the tilt axis, as studied recently by Wang (1988, 1989). Predictions of G_{disl} and G_{cleav} for the bicrystals tested were made by Wang and Anderson (1989) based on a formulation like in eq.(3.12) and with structural and segregation models for $2\gamma_{int}$. Behavior of the $\Sigma 9$ [110] symmetric tilt bicrystal, with $(2\bar{2}1)$ interfacial plane, is especially interesting. It can be cracked under tensile loading in a brittle manner along the interface when the direction of crack introduction is $[1\bar{1}4]$, but the interface does not crack and failure is instead ductile when the direction of attempted cracking is in the opposite direction, i. e., in the $[\bar{1}14]$ direction. Theoretical calculations based on

expressions like (3.12) have been shown (Anderson and Rice, 1986; Wang and Anderson 1989) to predict a much higher value of G_{disl} (under the same pure mode I loading) for the $[1\bar{1}4]$ cracking direction than for the $[\bar{1}14]$ direction; this is due to the different orientations of potentially relaxing slip systems relative to the crack tip in the two cases. Accordingly, the observed behavior can be explained as a case of G_{cleav} being reached before G_{disl} for the brittle $[1\bar{1}4]$ direction, but G_{disl} before G_{cleav} for the ductile $[\bar{1}14]$ direction. Thus, as Rice and Wang (1989) pointed out, it oversimplifies to say that an interface is intrinsically cleavable, because G_{disl} is not a fixed number for a given interface but depends on the direction of crack growth along it, as well as on the mixity of shear with tensile loading relative to the crack. Similar orientation and cracking direction dependence is to be expected for interfaces between dissimilar materials, such as typical metal/ceramic interfaces, and these effect are embodied by our expression in (3.8) for G_{disl} . We illustrate them in the next subsection in analysis of Cu/Al_2O_3 interfacial fracture specimens.

3.3 Application to single crystal Cu/sapphire interfaces. Consider a four-point bending specimen of a Cu single crystal bonded to a layer of sapphire (fig. 9a,b). The sapphire layer is notch cracked to the interface and a central crack continues along the interface. The Cu single crystal is oriented in all cases that we consider so that the crack fronts at both ends lie along the intersection of a pair of {111} slip planes of the Cu crystal with the interface; i. e., the crack tip lies along [110] in the Cu in all cases. This configuration allows application of the simple model developed in the preceding section, summarized as eqs. (3.8, 10, 11).

For simplicity, and because some of the solutions needed would not otherwise be available, we neglect the elastic anisotropy of the Cu and Al_2O_3 here. Both are treated as elastically isotropic, and we use averaged properties for each as in preparing Table I. The thickness h of the sapphire is assumed to be 1 mm in fig. 9a and b, and the ratio of Cu to sapphire thickness to be 0.3. Also, the crack length is assumed long enough for the analysis summarized by eq. (2.13) and fig. 7 to apply. For the present case, $\alpha = -0.47$ and $\varepsilon = 0.031$. From fig. 7c, $\psi = -52^o$ at the two crack tips in all cases (we reverse the signs of α, ε and ψ in reading fig. 7 since the 1 and 2 labelling of the materials is interchanged there; here 1 is Cu and 2 is Al_2O_3). Thus the phase angle ψ' of (3.10) relevant to crack tip events at the atomic scale is, since L = h for the definition of ψ in (2.13),

$$\psi' = \psi - \varepsilon \, ln \, (h/b) = -52^o - 0.031 \, ln \, (1mm/0.25nm) = -52^o - 27^o = -79^o \qquad (3.13)$$

This is a significant phase shift. (The effects of non-zero ε, and of the associated variable loading phase conditions near the crack tip, can often be neglected in engineering applications of interface fracture mechanics, as suggested by Hutchinson (1989), especially in a small ε situation like the present case. However, since we are here dealing with a process occurring at the atomic scale, the predicted shift of the phase angle (-27^o) relating to ε is significant and has some possibly testable consequences. The entire ε effect of consequence is, however, only in the shift of the phase angle; the small non-zero ε of 0.031 has negligible effect on the functions $\Sigma_{r\theta}(\theta)$, as can be seen from fig. 2.

Values of G_{disl} have been calculated from (3.11) for various crack tips in fig. 9, and results are summarized below. The favored of the two {111} slip planes passing through each tip is that on which

the combination involving ψ' in the denominator in (3.11) has the largest value; if ψ' is such that the combination is negative for both systems, then dislocations cannot be nucleated on them. We assumed that the dislocations nucleate in dissociated form and that the controlling event is the nucleation of the second partial. This is treated approximately by evaluating (3.11) with $\phi = 60^o$ and $r_c = b = 0.15$ nm for the partial (and with $\mu_1 = 5 \times 10^{10}$ N/m^2 and $\nu_1 = 0.3$ for Cu). We note that the comparison of (3.8) with (3.12) above suggests that the actual G_{disl} may be of order 50% higher than what we estimate from (3.11); also, G_{disl} is proportional to b/r_c, and the proper choice of core size r_c is quite uncertain. Thus the magnitudes that we report for G_{disl} should be taken in a somewhat qualitative sense, although their relative sizes in different cases will presumably correlate the ease of dislocation nucleation in those cases.

$(2\bar{2}1)_{Cu}$ *interface,* $[1\bar{1}4]$ *cracking direction (right-hand crack tip in fig. 9a).* The two slip planes which pass through the crack front are $(1\bar{1}1)$ and $(1\bar{1}\bar{1})$, with $\theta = 15.8°$ and 125.3°, respectively. Due to the large negative phase angle, -79°, for the crack tip field, shear stresses on only the $(1\bar{1}\bar{1})$ system are favorable for nucleation and we find from (3.11) that $G_{disl} = 0.86$ J/m^2.

$(2\bar{2}1)_{Cu}$ *interface,* $[\bar{1}14]$ *cracking direction (left-hand crack tip in fig. 9a).* The $(1\bar{1}\bar{1})$ and $(1\bar{1}1)$ planes are at $\theta = 54.7°$ and 164.2°, respectively, relative to the crack direction. The former is not favorably stressed for nucleation in the -79° near-tip loading phase, and the latter is favorably but only poorly stressed. Thus nucleation occurs on the $(1\bar{1}1)$ plane, but only at $G_{disl} = 4.9$ J/m^2.

Thus there is a more than factor-of-five difference between the G_{disl} values for the two directions of crack growth along the same $(2\bar{2}1)_{Cu}$ interface. If G_{cleav} for the interface lies in the broad range between 0.86 and 4.9 J/m^2, then dislocation blunting should occur at the right-hand crack tip in fig. 9a, whereas interfacial decohesion, unimpeded by dislocation nucleation, should occur at the left-hand tip. Even if G_{cleav} lies somewhat below that range, one should still expect strong differences in brittleness for the two cracking directions, since the different G_{disl} reflect different intensities of resolved shear stress along near-tip slip planes, which should also be important for the motion of pre-existing dislocations in the crystal lattice.

Thus we have reached the same conclusion for the bimaterial interfaces as that for metal bicrystal boundaries discussed above: It oversimplifies to say that an interface is intrinsically cleavable. The ductile vs. brittle response of an interface is expected theoretically to be crack direction dependent, and that expectation has been supported experimentally by Wang's (1989) results on symmetric [110] tilt Cu bicrystals, with $(2\bar{2}1)$ boundary plane, loaded in tension. That $(2\bar{2}1)$ boundary of Wang's bicrystal involves the same crystal plane as that just discussed as the interface for the Cu/sapphire layer combination in fig. 9a. Both cases lead to theoretical prediction of strong crack direction dependence. What is also remarkable, however, is that the brittle $[1\bar{1}4]$ direction for the tensile-loaded Cu bicrystal is the ductile direction for the Cu/sapphire composite loaded in bending and, conversely, the ductile $[\bar{1}14]$ direction for

the bicrystal in tension is the brittle direction for the composite in bending! This is all due to the distinctly different loading phase angles at the crack tips.

$(001)_{Cu}$ *interface,* $[\bar{1}10]$ *cracking direction (right-hand crack tip in fig. 9b), or* $[1\bar{1}0]$ *cracking direction (left-hand crack tip in fig 9b).* These two cases give identical G_{disl} because of the symmetry; there is no crack direction dependence for the two directions considered. At both crack tips $\theta = 54.7°$ and 125.3° for {111} slip planes through the tip. The first plane is not favorably stressed for nucleation, given the local -79° loading phase, but the latter is and one again finds $G_{disl} = 0.86$ J/m^2. Thus this interface is expected to be ductile (or comparatively ductile, if G_{cleav} is somewhat below 0.86 J/m^2) for both crack directions considered.

We can better understand this case with reference to fig. 10, in which G_{disl} as calculated from (3.11) is shown as a function of the atomic scale phase angle ψ' at the crack tip; the slip system on which the dislocation nucleates is also indicated. (For the $(2\bar{2}1)$ boundary of fig. 9a, a pair of such plots would be needed, one for each growth direction.) Evidently, the bending specimen of fig. 9b, with $\psi' = -79°$, coincides with a broad minimum in G_{disl}; other specimen designs, or other modes of stressing the crack tip, could lead to higher G_{disl} values and hence would be likely to show more brittle response. E. g., the most brittle case is when $\psi' = -15°$, for which case $G_{disl} = 3.5$ J/m^2. For Cu/sapphire specimens with characteristic dimensions of order 1 mm, that most brittle case occurs when the angle ψ as introduced in (2.4) is $\cong +12°$. Some results for other test specimens are as follows:

$(001)_{Cu}$ *interface, like in fig. 9b, but with the Cu and sapphire interchanged.* The configuration considered is like in fig. 7a, with 1 denoting Cu and 2 sapphire. One finds $\psi = 42°$ and thus $\psi' = 42° - 27° = 15°$, which corresponds to $G_{disl} = 1.42$ J/m^2.

$(001)_{Cu}$ *interface, along which a 1 mm sapphire layer is bonded to a 1.5 mm Cu crystal layer; wedging forces act normal to the surface of a long crack between them.* The different layer thicknesses are chosen to match bending resistance. This case has a phase $\psi \cong 0$; thus $\psi' \cong -27°$ and $G_{disl} \cong 1.94$ J/m^2; it should be much more brittle than the other specimens considered.

$(001)_{Cu}$ *interface as in fig. 9b; microcrack ahead of main crack as in fig. 9c.* The microcrack is treated for simplicity as a tunnel crack with center at distance r_m ahead of the macrocrack tip; its end B is closest to the macrocrack tip and end A grows in the same direction as the macrocrack. The important factor is that the atomic scale phase angle ψ' is different at the two ends A and B of the microcrack, so G_{disl} is different too. We estimate ψ' at B by regarding the microcrack as a crack of length 2a under a remotely uniform stress field, like in eq.(2.9) and fig. 3; that remote stress field is equated to the local stress which would have acted at distance r_m ahead of the macrocrack tip (i. e., at the center of the microcrack) if the microcrack were not present. Thus, since the concern is with tip B, the $\sigma^{\infty}_{yy} + i\ \sigma^{\infty}_{yx}\ \left(= T\, e^{i\omega} \right)$ for use in (2.9) is chosen as $\sigma_{yy} - i\ \sigma_{yx}$ as would exist along the interface at

distance r_m ahead of the macrocrack tip if the microcrack were absent. Thus the phase ω of (2.9) $= -\psi + \varepsilon\, ln(h/r_m)$, where $\psi = -52^o$ as before from the bending analysis based on fig. 7. Therefore the atomic scale phase ψ' at B is, from (2.9) and (3.10) with L taken as 2a in the latter, $\psi' = \omega + 2\varepsilon - \varepsilon\, ln\ (2a/b) = -\psi - \varepsilon\, ln\ (2ar_m/hb)$. Choosing h and b as in (3.13) and assuming $r_m = 10\mu m$ and $2a = 5\mu m$ gives $\psi' = 52^o - 6^o = 46^o$ and $G_{disl} = 1.19\ J/m^2$ (increasing or decreasing both r_m and 2a by a factor of 5 decreases or increases ψ' by about 6^o but has little effect because the range is near the broad relative minimum for G_{disl} at positive ψ' in fig. 10). A similar analysis gives $\psi' = -74^o$ and $G_{disl} = 0.86\ J/m^2$ at end A of the microcrack, close to the result for macrocrack tip C. It fortuitously turns out for the configuration of figs. 9b,c that all crack tips map close to minima in the G_{disl} *vs.* ψ' relation, but that for end B is about 40% higher which is consistent with more brittle behavior at B.

While we do not pursue it here, it is possible to find configurations for which there is strongly different behavior predicted at the two ends of such a microcrack, as hinted by the variations in fig. 10. In cases for which a substantially higher G_{disl} is found at end B, we may expect that macroscopic fractures could occur by microcracks forming ahead of the main crack and propagating backwards to join up with it.

$(001)_{Cu}$ *interface in specimen of shape like in fig. 9b, but with Cu in the form of a 25 μm film bonded to sapphire on both sides.* The upper part of the bend specimen in fig. 9b as well as the notched layer at the bottom are sapphire in this case; the Cu is present only as a thin sandwich-like film. This configuration is similar to an experimental arrangement by Evans (1989) and coworkers on an Au film between sapphire layers. We may use the analysis from fig. 7 to find the classical K_I and K_{II} at the macrocrack tip when there is no sandwich; their phase angle is -46^o. Using the sandwich solution of figure 6, one then determines that the phase $\psi = -39^o$ based on characteristic length L equal to the 25 μm sandwiched layer thickness. Thus the atomic scale phase $\psi' = -59^o$ at the main crack tip C, and $G_{disl} = 0.93\ J/m^2$ there. If we again assume that a microcrack exists ahead of the main crack, like in fig. 9c, the phase angle at distance $r_m = 10\ \mu m$ in the absence of that microcrack would then be -41^o. Proceeding as above with the same microcrack size one finds $\psi' = 27^o$ at microcrack tip B, so that $G_{disl} = 1.21\ J/m^2$ there, and $\psi' = -55^o$ so that $G_{disl} = 0.97\ J/m^2$ at tip A. Again, tip B is predicted to be more brittle than A, although the difference is smaller in this case.

Based on measurement of the contact angle between Al_2O_3 particles and a Cu matrix at high temperature, it was reported (Nicholas, 1968) that the work of adhesion $W_{ad} = 0.475\ J/m^2$. This value may be taken as an approximation to $2\gamma_{int}$ for the Cu/sapphire interface at room temperature. If it is correct, and if there are no strong lattice trapping effects, then our estimates of G_{disl} above suggest $G_{cleav} < G_{disl}$ for even the most ductile Cu orientations considered, and the interface is intrinsically cleavable. Still, the differences in G_{disl} for different cases signal different amounts of shear stress resolved onto near tip slip systems and, as mentioned, G_{disl} is therefore still expected to correlate with the relative brittleness of response.

4. Effect of Solute Segregation on Interfacial Embrittlement

We review briefly studies of impurity segregation at ceramic and metal/ceramic interfaces and then close with discussion of thermodynamic interrelations between adsorption at interfaces and the ideal work $2\gamma_{int}$ of their brittle separation. For the latter discussion, the thermodynamic framework of Rice (1976) and Hirth and Rice (1980), as used recently by Rice and Wang (1989) and Anderson et al. (1989) in analysis of intergranular embrittlement of Fe-base alloys, is stated in a manner appropriate to interfaces between dissimilar solids, e. g., to metal/ceramic interfaces. Impurity segregation may reduce or enhance $2\gamma_{int}$ depending on the relative propensity of segregation to the interface *vs.* to the pair of surfaces which result after separation. *Normal* segregators locate more abundantly, at a given equilibrating potential, on the pair of surfaces resulting from fracture than on the unstressed interface, and because of that they cause $2\gamma_{int}$ to decrease. *Anomalous* segregators instead locate more abundantly at the unstresssed interface; they increase $2\gamma_{int}$.

4.1 Review of solute segregation at ceramic and metal/ceramic interfaces. Impurity segregation in metals and their alloys has been studied extensively. It can convert a ductile alloy to one which cracks in a brittle manner along grain interfaces and, in some cases, can ductilize an alloy which is otherwise intergranularly brittle. The scope for impurity-induced alteration is presumably less broad in the more inherently brittle ceramic and metal/ceramic systems, and perhaps for that reason the phenomenon is less studied in those cases.

One well investigated case is Ca segregation at grain boundaries in MgO-doped or NiO-doped Al_2O_3. Stein and Johnson (1975) and Marcus and Fine (1972) observed that the Ca^{+2} ion segregated to the grain boundaries, but Ni and Mg did not. The driving force was argued to be the elastic strain energy produced by the size misfit between Ca^{+2} and Al^{+3} cations. The Langmuir-McLean type isotherm was found to be valid for the Ca^{+2} segregation and a segregation free energy of $\Delta g_b^0 = -121$ kJ/mole in the temperature range 1700 - 1900°C was reported. Jupp and Smith (1980) observed that segregation of CaO at Al_2O_3 grain boundaries reduces the fracture toughness and promotes intergranular fracture, and Funkenbusch and Smith (1975) suggested that Ca^{+2} segregation reduces the cohesive strength of Al_2O_3 grain boundaries. Interfacial embrittlement was also observed in SiC with Al_2O_3 as segregant (Tajima and Kingery 1982) and SiC fiber reinforced lithium-aluminosilicate glasses and glass-ceramics with as Nb_2O_3 segregant (Brennan 1986).

The mechanisms of embrittlement of ceramics by segregation sometimes involves forming an interfacial phase. Faber et al (1988) found that LiF additions to MgO results in a grain boundary phase which causes embrittlement, but this does not seem to apply for Ca^{+2} segregation in Al_2O_3 since no second phase is found. In order to understand the effect of atomic level segregation on the cohesive strength of interfaces, attention must be paid also to the energetics of the segregant on surfaces of the type formed by fracture. The interfacial fracture process in brittle materials is merely a process of separating the interface to produce two free surfaces, and the thermodynamic formalism to follow makes it evident that segregant properties in the final state (the two separated free surfaces) are equally as important as are those

of the initial state (the impurity segregated interface) to understanding the phenomenon. There seems to be rather little work done on surface segregation for ceramic materials.

Fischmeister et al (1972) noted that alloying additions could have a marked effect on the contact angle between oxide particles and liquid metals, and thus on the work of adhesion, and that a similar effect of alloying on interfacial energy would be likely to occur in the solid state. They showed that particle/matrix bonding in the Al_2O_3 dispersion strengthened Ni-base and Fe-base alloys was largely dependent on the magnitude of the interfacial energy between the oxide and the metal, which in turn was dependent on matrix alloying. The affects could be positive or negative. It is likely that alloying additions affect the bonding energy at least in part through their effect on impurity segregation behavior.

Segregation at the interfaces between metals and scales, which form on the metal surface during high temperature exposure in an oxidizing atmosphere, received great attention in the development of high temperature alloys . Bonding between Cr_2O_3 and Al_2O_3 scales and metals is basically strong and it is weakened by S segregation at the interfaces. Reactive elements such as Y, Hf and Zr, and dispersions of their oxides improve bonding by preventing S from segregating to the interfaces (Melas et.al. 1988, Smialek, 1987, Smeggil, 1987 and Funkenbusch et al 1985). Recently, Stott (1988) reviewed scale/metal bond strengths and the methods of improving adherence. Besides S, small quantities of Cu, Sn, As, Sb or P can segregate to the scale/metal interface, giving a reduced scale adherence, while Y and Zr can enhance the scale adherence. This enhancement of the adherence may be due to the eliminating of the impurity segregation or due to the segregation of the reactive elements themselves to the oxide/metal interface.

Intergranular fracture of homogeneous materials produces two free surfaces of the same type (although of generally different crystal faces) between which the segregated atoms, or ions in the case of ceramics, can be assumed to divide approximately equally. Debonding of metal/ceramic interfaces produces a metal surface and a ceramic surface, and the thermodynamic properties and distributions of the segregant on these surfaces will in general be different from each other. As mentioned, understanding this final state of interfacial separation is extremely important in understanding the embritttling (or ductilizing) effects of segregation.

4.2 Thermodynamics of interfacial separation. With reference to fig. 11, we focus on the interface as a thermodynamic system which is assumed to be in local equilibrium but which may be (and typically is, at low temperatures) out of composition equilibrium with adjoining bulk solid phases, both before and after separation. Interfacial thermodynamic quantities are defined as Gibbs-like excesses relative to those of the two adjoining phases.

We deal exclusively with solutes which are far more abundant along the interface than in a few atomic layers, well removed from the interface, in either adjoining phase. In that case Γ^i, the concentration of segregant i per unit area of interface, is well defined and we assume that an equilibrating chemical potential μ^i can be associated with each segregating species i as it exists at the interface. This is illustrated for a single segregant, represented by black dots, in figs. 11 and 12.

Thus, where u and s are the excesses of energy and entropy per unit area of interface, in a formulation which treats the interface region as being constrained against the necessity of solute composition equilibrium with the adjoining solid phases, one has

$$du = Tds + \sigma_{yy}d\delta_y + \sigma_{yx}d\delta_x + \sigma_{yz}d\delta_z + \sum_i \mu^i d\Gamma^i \qquad (4.1)$$

for reversible changes of state.

The key assumption, embedded in the above equation, is that all thermodynamic functions referring to the interface, e.g., u, s, the $\sigma_{y\alpha}$ and the μ^i, are determined by the values of T, the δ_α and the Γ^i, regardless of the solute concentrations (say, c_1, c_2 ...) in the adjoining phases. If (4.1) holds throughout a separation process (one in which δ_y is increased toward indefinitely large values) as assumed in the present modelling, then any distinction is neglected between the pair of free surfaces resulting from such a decohesion fracture and free surfaces having the same T and Γ^i, but produced by a different thermal/mechanical route. The latter route might, e.g., have involved equilibrium solute segregation to the free surfaces at a higher temperature and, possibly, a surface reconstruction.

The work of separation is

$$2\gamma_{int} = \int_{initial}^{final} (\sigma_{yy}d\delta_y + \sigma_{yx}d\delta_x + \sigma_{yz}d\delta_z) \qquad (4.2)$$

where the *initial* state is an unstressed interface (all the $\sigma_{y\alpha} = 0$) and the *final* state is a pair of fully separated surfaces.

Note that in the initial and final states the properties of the interface (or of the pair of free surfaces that it became) depend only on T and the equilibrating potentials μ^i of the segregants. Note that for consistency in deriving consequences of eq. (4.1), one must assume that the segregants distribute between the two separated surfaces, 1 and 2, so that those surfaces are in composition equilibrium with one another (i. e., both surfaces are equilibrated by the same set of μ^i); that is because the formulation assumes that local equilibrium holds within the interface region during separation. Thus the Γ^i in the final state always are to be understood as the total amount i per unit area associated with both fracture surfaces, its distribution between the two being understood to be however necessary as to give identical equilibrating μ^i for both surfaces. The issue did not come up explicitly in previous applications of the formalism of Rice

(1976) and Hirth and Rice (1980) to fracture of interfaces between identical solids, although in that case the equilibrium requirement is met implicitly through assuming that the solutes distribute equally between the pair of surfaces created by the fracture. Of course, the dynamics of actual interfacial fractures, especially those which occur rapidly, may sometimes be such that the two fracture surfaces are well out of composition equilibrium with one another. However, following an argument by Rice (1987) based on the second thermodynamic law, one may show that any such separation process requires more work than what we calculate as the work of separation by assuming composition equilibrium between the two surfaces.

When dealing with initial and final states we use the following system of subscripts: *1/2* denotes the unstressed interface between solids 1 and 2; *s,1* denotes the surface of solid 1 after fracture and *s,2* denotes the surface of 2 after fracture; when we refer to a property of the pair of surfaces after fracture we use subscript *fin* (for *final* state). Thus the adsorption behavior of the interface at fixed T is described with the notations $\Gamma^i = \Gamma^i_{1/2}(\mu^1, \mu^2, \mu^3,...)$ for i = 1,2,3,..., with inverses $\mu^i = \mu^i_{1/2}(\Gamma^1, \Gamma^2, \Gamma^3,...)$. Such a relation for a single segregant of amount Γ and equilibrating potential μ is sketched in fig. 12 as the curve $\Gamma = \Gamma_{1/2}(\mu)$. The similar relations for the pair of surfaces resulting after fracture are $\Gamma^i = \Gamma^i_{fin}(\mu^1, \mu^2, \mu^3,...)$ and their inverses are $\mu^i = \mu^i_{fin}(\Gamma^1, \Gamma^2, \Gamma^3,...)$. Given that each μ^i is the same for both the fracture surfaces, the functions Γ^i_{fin} can be calculated directly from the adsorption isotherms for the surfaces taken individually. Letting Γ^i_1 denote the amount of i on the fracture surface of solid 1, the adsorption isotherms for that surface have the form $\Gamma^i_1 = \Gamma^i_{s,1}(\mu^1, \mu^2, \mu^3,...)$, i = 1,2,3,... , and similarly for surface 2.. Thus noting that $\Gamma^i = \Gamma^i_1 + \Gamma^i_2$, when referring to a pair of surfaces, we see that the functions Γ^i_{fin} are given by

$$\Gamma^i_{fin} = \Gamma^i_{s,1}(\mu^1, \mu^2, \mu^3,...) + \Gamma^i_{s,2}(\mu^1, \mu^2, \mu^3,...) \qquad (4.3)$$

The adsorption isotherm in fig. 12 corresponding to the pair of free surfaces has been labelled accordingly, that is, the function $\Gamma = \Gamma_{fin}(\mu)$ marking that isotherm has been written as $\Gamma = \Gamma_{s,1}(\mu) + \Gamma_{s,2}(\mu)$.

The work expression of (4.2) is assured by eq. (4.1) to be independent of path in the δ_α space in the special cases when s (or T) and the Γ^i (or the μ^i) are held constant, although we noted earlier the possibilities that irreversibilities could occur, as local instabilities equivalent to sudden introduction of dislocations along the interface, when shear accompanies opening as inevitably so for elastically dissimilar materials. More generally, on the reversible paths which we assume, the integral does not define a unique value until one characterizes the variation (if any) of T and the Γ^i with the δ_α during separation. We regard T as constant during separation here and consider, like in Rice (1976) and Hirth and Rice (1980), the two cases which follow.

Separation at fixed solute composition. In the first case the Γ^i are all assumed to remain fixed in amount during separation , which is the normal case at low T and with non-mobile segregants

$$(2\gamma_{int})_{\{\Gamma\}=\text{const}} = f_{fin}(\{\Gamma\}) - f_{1/2}(\{\Gamma\}) = f_{s,1}(\{\Gamma_1\}) + f_{s,2}(\{\Gamma_2\}) - f_{1/2}(\{\Gamma\}) \qquad (4.4)$$

Here f = u − Ts is the excess Helmholtz free energy per unit area and, in the latter form it is to be remembered that $\{\Gamma\}$ is fixed so that $\{\Gamma_1\}$ and $\{\Gamma_2\}$ must satisfy $\{\Gamma\} = \{\Gamma_1\} + \{\Gamma_2\}$ and assure that $\mu^i_{s,1} = \mu^i_{s,2}$ for each segregant. (The $\{\Gamma\}$ is a shortened notation for the set $\Gamma^1, \Gamma^2, \Gamma^3, \ldots$.) Thus, following Rice (1976), or more simply Hirth and Rice (1980) in considering separate-desorb-rejoin-adsorb cycles, it follows from (4.1) that

$$(2\gamma_{int})_{\{\Gamma\}=\text{const}} = (2\gamma_{int})_0 - \int_{\{0\}}^{\{\Gamma\}} \sum_i [\, \mu^i_{1/2}(\{\Gamma\}) - \mu^i_{fin}(\{\Gamma\}) \,]\, d\Gamma^i \tag{4.5}$$

where $(2\gamma_{int})_0$ is the work to separate a clean interface (with $\{\Gamma\} = \{0\}$). For the case of a single segregant the reduction of $2\gamma_{int}$ from $(2\gamma_{int})_0$ is marked as an area in fig. 12. Eq. (4.5) links $2\gamma_{int}$, for separation at fixed composition, to quantities which can, in principle, be estimated from solute segregation studies. When the interface and surface coverages are less than values corresponding to full coverage of a set of adsorption sites, idealized as well as having the same low energy relative to solute sites in the bulk, the simple Langmuir-McLean model (McLean, 1957) may be adopted. Thus, considering a single segregant of amount Γ ($= \Gamma_1 + \Gamma_2$ on the pair of fracture surfaces)

$$\mu_{1/2}(\Gamma) = \Delta g^o_{1/2} + RT\, ln\, [\Gamma / (\Gamma^o_{1/2} - \Gamma)]$$
$$\mu_{s,1}(\Gamma_1) = \Delta g^o_{s,1} + RT\, ln\, [\Gamma_1 / (\Gamma^o_{s,1} - \Gamma_1)] \;,\; \mu_{s,2}(\Gamma_2) = \Delta g^o_{s,2} + RT\, ln\, [\Gamma_2 / (\Gamma^o_{s,2} - \Gamma_2)] \tag{4.6}$$

where the (inherently negative) Δg^o terms are referenced to a bulk phase at the same T, i.e., are based on the expression $\mu = RT \ln [c / (1-c)] \approx RT \ln c$ for the equilibrating potential when a fraction c of available solute sites are occupied in the bulk, the Γ^o's are the full coverages for the interface and fracture surfaces, respectively. The Δg^o terms have the form $\Delta h - T\Delta s^o$, where the Δh terms are the enthalpies of segregation (essentially identical to energies of segregation in the present context since pressure times volume terms are negligible for the unstressed boundary and free surface), and the Δs^o terms are entropies of segregation relating to changes in the atomic vibrational spectrum.

For separations at fixed composition, if the initial coverage (labeled Γ_o in fig. 12) on the interface falls within the Langmuir-McLean range, then the coverages Γ_1 and Γ_2 on the separated surfaces are also likely to do so and the equations above for the μ can be used directly in the calculation of $2\gamma_{int}$. Following a comparison of the order of different terms like in Rice and Wang (1989), the configurational entropy terms make little contribution to the integral in (4.5) at low T, say, T = 300 K, and thus

$$(2\gamma_{int})_{\Gamma=\Gamma_o} \;\cong\; (2\gamma_{int})_0 - [\, \Delta g^o_{1/2}\, \Gamma_o - \Delta g^o_{s,1}\, \Gamma_1 - \Delta g^o_{s,2}\, \Gamma_2 \,] \tag{4.7}$$

Here Γ_1 and Γ_2 are determined from the equations $\Gamma_1 + \Gamma_2 = \Gamma_o$ and $\mu_{s,1} = \mu_{s,2}$ in the second line of (4.6). What the latter enforces at low T is that essentially all the solute go to the fracture surface with the smallest (i. e., largest in absolute value) value of Δg^o, at least until the capacity Γ^o for that surface is reached, and then go to the other surface. Eq.(4.7) is consistent with the results of Smith and Cianciolo (1989), who also consider bimaterial interfaces with impurity segregation.

Data for $\Delta g^{o}_{s,1}$, where 1 denotes the metal in a metal/ceramic 1/2 interface, can be found in the literature (e.g. for impurities in Fe and Fe alloys, as summarized by Rice and Wang (1989)). Data for ceramic surfaces are limited. It is expected that segregators are normally situated more abundantly on a pair of free surfaces than on an unstressed interface, which means that the combination of terms within the bracket in (4.7) are positive (we remind that the Δg^{o}'s are intrinsically negative), and that the interface and fracture surfaces adsorption isotherms are situated relative to one another like in fig. 12. In this case, $2\gamma_{int} < (2\gamma_{int})_0$, the cohesive energy of the interface is reduced by segregation. This might be the case of segregation of S at the metal/oxide interfaces, and is likely also the case for Cu, Sn, As, Sb and P segregation.

Nevertheless, thermodynamics does not preclude the existence of anomalous segregators for which the above inequalities are reversed. Such anomalous segregators increase $2\gamma_{int}$ and hence are expected to increase interfacial toughness. Y and Hf may possibly be examples of anomalous segregators; we mentioned earlier that they enhance the cohesive strength of the metal/oxide interface, although other mechanisms, such as site competition or impurity gettering, are also possible.

Separation at fixed potential of a mobile segregant. While separation at fixed composition seems to be the normal failure mode in low temperature debonding processes, it is useful to consider an opposite limiting case. This limit is separation at constant potential μ ($= \mu_o$, say) implying that there is (for "normal" segregators) solute inflow to the interface region during separation so as to maintain μ fixed, e.g., at the value for an adjoining bulk phases with which there is composition equilibrium. Such conditions require mobility. They are probably met approximately in low temperature hydrogen assisted cracking of some interfaces. They may be met also in high T debonding of metal/scale interfaces.

The μ = const. = μ_o path is also shown in fig. 12. The initial state is $\Gamma = \Gamma_o$ and $\mu = \mu_o$. For separations at fixed μ the relevant thermodynamic function is $\gamma = f - \mu\Gamma$, and

$$(2\gamma_{int})_{\mu = const} = \gamma_{fin}(\mu) - \gamma_{1/2}(\mu) = \gamma_{s,1}(\mu) + \gamma_{s,2}(\mu) - \gamma_{1/2}(\mu) \tag{4.8}$$

Also, following Rice (1976),

$$(2\gamma_{int})_{\mu = \mu_o} = (2\gamma_{int})_0 - \int_{-\infty}^{\mu_o} [\Gamma_{s,1}(\mu) + \Gamma_{s,2}(\mu) - \Gamma_{1/2}(\mu)]\, d\mu \tag{4.9}$$

This result for the alteration of $2\gamma_{int}$ can be interpreted graphically as the sum of the two areas marked in fig. 12. Segregant coverages on a single metal and ceramic free surfaces, and on an interface, at equilibrating potential μ, can be calculated from (4.6) in the range where the Langmuir-McLean model applies.

The difference in $2\gamma_{int}$ at constant Γ *vs.* that at constant μ can be numerically significant. Examples given by Anderson et al. (1989) for H and (at higher temperature) S on Fe grain boundaries show that

substantial reductions of $2\gamma_{int}$, of order 0.5 $(2\gamma_{int})_0$, can occur in separations at constant μ, under potentials μ that are so low that they equilibrate negligible Γ on the unstressed interface, and hence would involve $2\gamma_{int} \cong (2\gamma_{int})_0$ in rapid separation at constant Γ. This shows that mobility (or slowness of the attempted separation) is a factor which worsens the already deleterious effect of a normal segregator on $2\gamma_{int}$. It also reduces the beneficial effect of an anomalous one. We emphasize again that embrittlement or toughening, at least as it mirrors $2\gamma_{int}$, is always seen to depend on differences between segregant effects on the initial interface and on the two free surfaces created by the fracture. Thus a focus on the electronic alterations induced by segregants in interface, without corresponding study of what they induce on free surfaces, is unlikely to be definitive in explaining solute embrittlement. The differences in energy and entropy between the two states are of primary interest.

Acknowledgement

We gratefully acknowledge J.W. Hutchinson for discussions on section 2 of the paper and D. Shum for commenting on a portion of the manuscript. Support was provided at Harvard University through sub-agreement VB38639-0 with the University of California at Santa Barbara, based on the Office of Naval Research contract N00014-86-K-0753, and also for JRR through the Fairchild Scholars program at the California Institute of Technology.

References

Anderson, P. M. (1986), *Ductile and brittle crack tip response*, Ph. D. Thesis, Harvard University

Anderson, P. M. (1988), *J. Appl. Mech.*, **55**, 814.

Anderson, P. M., and J. R. Rice (1986), *Scripta Metall.*, **20**, 1967.

Anderson, P. M., J.-S. Wang and J. R. Rice (1989), "Thermodynamic and mechanical models of interfacial embrittlement", in *Proc. Sagamore Conf. on Innovations in High Strength Steel Technology*, edited by M. Azrin, G.B. Olson and E. S. Wright, in press.

Argon, A.S., V. Gupta, H. S. Landis, J. A.and Cornie (1989), *J. Mater. Sci.*, **24**, 1406-1412.

Bassani, J. L. and J. Qu (1989), *Mat. Sci. and Eng.* **A107**, 177.

Brennan, J. J. (1986), in *Tailoring Multiphase and Composite Ceramics*, edited by R. E. Tressler, G. L. Messing, C. G. Pantano and R. E. Newnham (Plenum Press, New York,), p. 549.

Cao, H.C. and A. G. Evans (1989), "An experimental study of the fracture resistance of bimaterial interface", *Mech. Mater.*, in press

Charalambides, P.G., J. Lund, A. G. Evans and R. M. McMeeking (1989a), *J. Appl. Mech.*, **56**, 77-82.

Charalambides, P.G, H. C. Cao, J. Lund and A. G. Evans (1989b), "Development of a test method for measuring the mixed mode fracture resistance of bimaterial interfaces", *Acta Met.*,to be published.

Comninou, M. (1977), *J. Appl. Mech.* **44**, 631 and 780.

Comninou, M. and D. Schmueser (1979), *J. Appl. Mech.* **46**, 345.

Dundurs, J. (1968), in *Mathematical Theory of Dislocations*, ASME, New York.

Evans, A. G (1989), privite communication.
Faber, K. T., and C. C. Hickenbottom (1988), in *Interfacial Structure, Properties and Design*, edited by M. H. Yoo, W. A. T. Clark and C. L. Briant, (MRS Vol.122), p. 475.
Fischmeister, H. F., E. Navara and K. E. Easterling (1972), *Met. Sci. J.* **6**, 211.
Funkenbusch, A. W., J. G. Smeggil and N. S. Bornstein (1985), *Metall. Trans.* **16A**, 1164.
Gao, H. and J. R. Rice. (1989), *J. Mech. Phys. Solids*, **37**, 155-174.
Hirth, J. P., and J. R. Rice (1980), *Metall. Trans.* **11A**, 1502.
Hirth, J. P. and J. Lothe (1982), *Theory of Dislocations*, 2nd Ed., John Wiley & Sons, New York.
Hutchinson, J. W.(1989), "Mixed mode fracture mechanics of interfaces", *Scripta Met.*, in press.
Jupp, R. S., and D. W. Smith (1980), *J. Mater. Sci.* **15**, 96.
Kelly, A., W. Tyson and A. Cottrell (1967), *Phil. Mag.*, **15**, 567.
Liechti, K. M. and E. C. Hanson (1988), *Int. J. Fracture* **36**, 199.
Marcus, H. L., and M. E. Fine (1972), *J. Amer. Cer. Soc.***55**, 568.
Mason, D. D. (1979), *Phil. Mag.* **39**, 455.
McLean, D. (1957), *Grain Boundaries in Metals*, Oxford University Press, Oxford.
Melas, I., and D. G. Lees (1988), *Mater. Sci. and Tech.* **4**, 455.
Nicholas, M. (1968), *J. Mat. Sci.*, **3**, 571.
Oh, T.S., R. M. Cannon and R. O. Ritchie (1987), *J. Am. Ceram. Sco.* **70**, C-352.
Rice, J. R. (1976), in *Effect of Hydrogen on Behavior of Materials*, edited by A. W. Thompson and I. M. Bernstein, TMS-AIME, p. 455.
Rice, J.R., (1985), in *Fundamentals of Deformation and Fracture* (Eshelby Memorial Symposium), Cambridge University Press, p. 33.
Rice, J. R. (1987) in *Chemistry and Physics of Fracture*, edited by R. M. Latanision and R. H. Jones, Martinus Nijhof Publishers, Dordrecht, p. 23.
Rice, J.R., (1988), *J. Appl. Mech.* **55**, 98.
Rice, J. R. and R. Thomson (1974), *Phil. Mag.*, **29**, 73.
Rice, J. R., and J.-S. Wang (1989), *Mater. Sci. Eng.* **A107**, 23.
Smeggil, J. G. (1987), *Mater. Sci. Eng.* **87**, 261.
Smialel, J. L. (1987), *Metall. Trans.* **18A**, 164.
Smith, J., and T. V. Cianciolo (1989), *Surface Sci.* **210**, L229.
Stein, D. F., and W. C. Johnson (1975), *J. Amer. Cer. Soc.* **58**, 485.
Stott, S. H. (1988), *Mater. Sci. Technol.* **4**, 431
Suga, T., E. Elssner and S. Schmauder (1988), *J. Composite Materials*, **22**, 917.
Suo, Z.(1989a), *Mechanics of interface fracture*, Ph. D. Thesis, Harvard University.
Suo, Z.(1989b), "Singularities interacting with interfaces and cracks", *Int. J. Solids. Structures*, in press
Suo, Z. (1989c), "Singularities, interfaces and cracks in dissimilar anisotropic media", *Harvard University Report Mech-137*, submitted to *Proc. Roy. Soc. Lond. A.*
Suo, Z. and J. W. Hutchinson (1989a), "Interface crack between two elastic layers", *Int. J. Fracture*, in press.
Suo, Z. and J. W. Hutchinson (1989b), *Mater. Sci. Eng.* **A107**, 135.
Tajima, Y., and W. D. Kingery (1982), *J. Mater. Sci.* **17**, 2289.

Thomson, R. (1983), in *Atomistics of Fracture*, edited by R. M. Latanision and J. Pickens, Plenum Press, New York, p. 167.

Thomson, R. (1986), in *Solid State Physics*, edited by H. Ehrenreich and D. Turnbull, Vol. 39, p.1.

Wang, J.-S. (1988), in *Interface Structure, Properties and Design*, edited by M. H. Yoo, C. L. Briant and W. A. T. Clark, MRS Vol. 122, p. 367.

Wang, J.-S. (1989) "Fracture behavior of embrittled f.c.c. metal bicrystals and its misorientation dependence (part 1. experimental)", submitted to *Acta Metall.*

Wang, J. - S. and P. M. Anderson (1989), "Fracture behavior of embrittled f.c.c. metal bicrystals and its misorientation dependence (part 2. theory and analysis)", submitted to *Acta Metall.*

Wang, J. - S., P. M. Anderson and J. R. Rice (1987), in *Mechanical Behavior of Materials -V*, edited by M. G. Yan, S. H. Zhang and Z. M. Zheng, Pergamon Press, p. 191

Wu, K.- C. (1989) "Stress intensity factor and energy release rate for interfacial cracks between dissimilar anisotropic materials", to appear in *J. Appl. Mech.*

Appendix: Angular Functions of the Near-Tip Fields for Joined Isotropic Solids

Listed below are angular functions of eq.(2.1) within for material 1 for modes I and II. For material 2, simply change π to $-\pi$ everywhere. The mode III functions are the same as for a homogeneous solid. A derivation using the Muskhelishvili potentials can be found in Rice (1988).

$$\Sigma^{I}_{rr} = -\frac{\sinh \varepsilon(\pi-\theta)}{\cosh \pi\varepsilon}\cos\frac{3\theta}{2} + \frac{e^{-\varepsilon(\pi-\theta)}}{\cosh \pi\varepsilon}\cos\frac{\theta}{2}(1+\sin^2\frac{\theta}{2}+\varepsilon\sin\theta)$$

$$\Sigma^{I}_{\theta\theta} = \frac{\sinh \varepsilon(\pi-\theta)}{\cosh \pi\varepsilon}\cos\frac{3\theta}{2} + \frac{e^{-\varepsilon(\pi-\theta)}}{\cosh \pi\varepsilon}\cos\frac{\theta}{2}(\cos^2\frac{\theta}{2}-\varepsilon\sin\theta)$$

$$\Sigma^{I}_{r\theta} = \frac{\sinh \varepsilon(\pi-\theta)}{\cosh \pi\varepsilon}\sin\frac{3\theta}{2} + \frac{e^{-\varepsilon(\pi-\theta)}}{\cosh \pi\varepsilon}\sin\frac{\theta}{2}(\cos^2\frac{\theta}{2}-\varepsilon\sin\theta)$$

$$\Sigma^{II}_{rr} = \frac{\cosh \varepsilon(\pi-\theta)}{\cosh \pi\varepsilon}\sin\frac{3\theta}{2} - \frac{e^{-\varepsilon(\pi-\theta)}}{\cosh \pi\varepsilon}\sin\frac{\theta}{2}(1+\cos^2\frac{\theta}{2}-\varepsilon\sin\theta)$$

$$\Sigma^{II}_{\theta\theta} = -\frac{\cosh \varepsilon(\pi-\theta)}{\cosh \pi\varepsilon}\sin\frac{3\theta}{2} - \frac{e^{-\varepsilon(\pi-\theta)}}{\cosh \pi\varepsilon}\sin\frac{\theta}{2}(\sin^2\frac{\theta}{2}+\varepsilon\sin\theta)$$

$$\Sigma^{II}_{r\theta} = \frac{\cosh \varepsilon(\pi-\theta)}{\cosh \pi\varepsilon}\cos\frac{3\theta}{2} + \frac{e^{-\varepsilon(\pi-\theta)}}{\cosh \pi\varepsilon}\cos\frac{\theta}{2}(\sin^2\frac{\theta}{2}+\varepsilon\sin\theta)$$

Also, $\Sigma_{zr} = \Sigma_{z\theta} = 0$ for these modes, and $\Sigma_{zz} = \nu(\Sigma_{rr} + \Sigma_{\theta\theta})$.

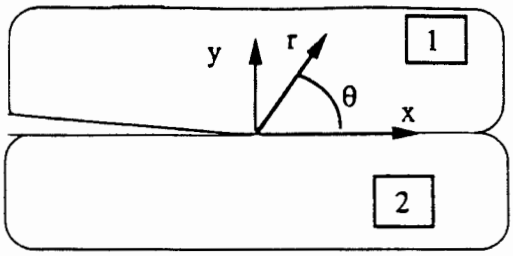

Fig. 1 Notation for an interface crack.

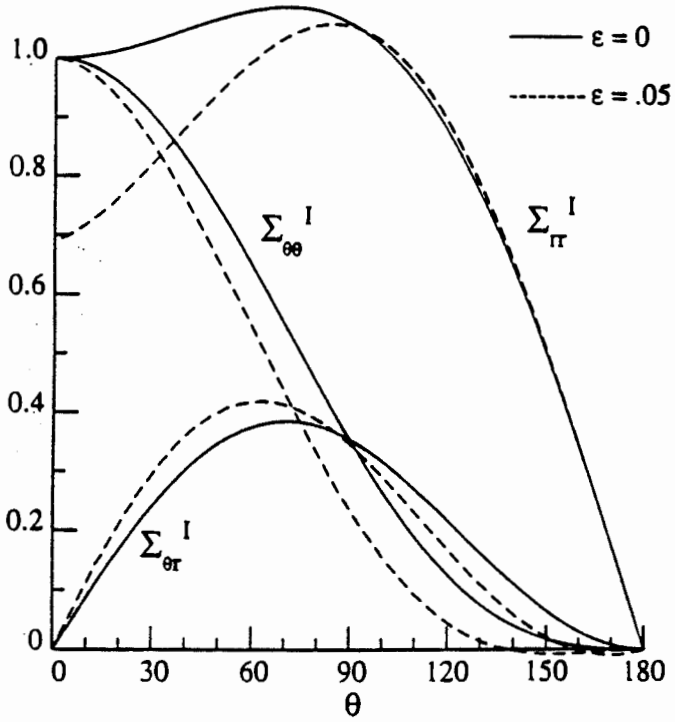

Fig. 2a Angular functions; mode I

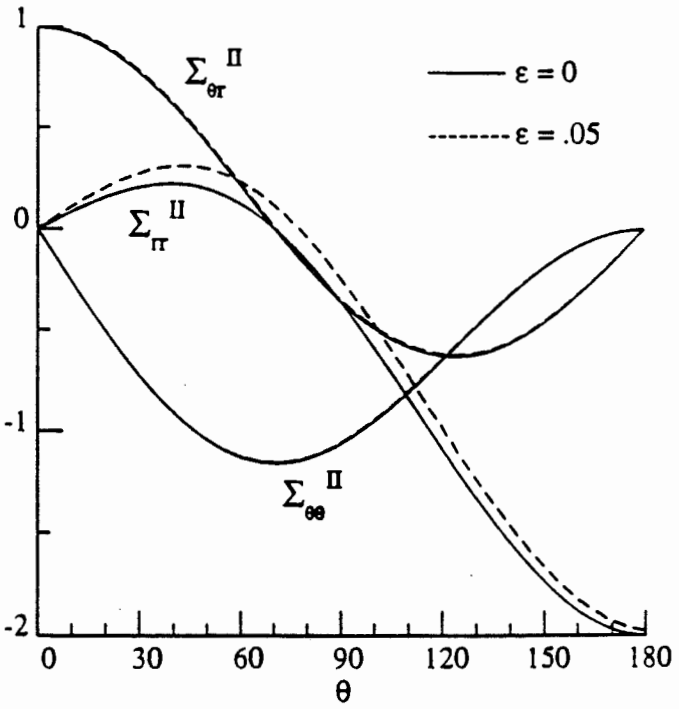

Fig. 2b Angular functions; mode II

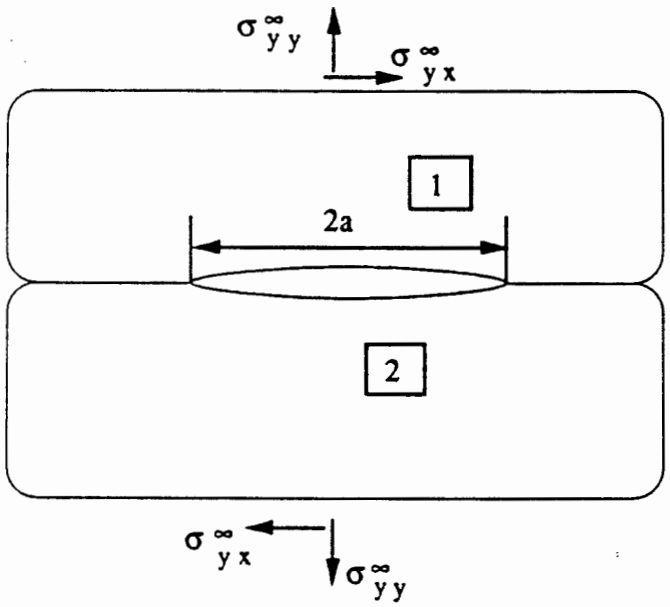

Fig. 3 An internal interface crack

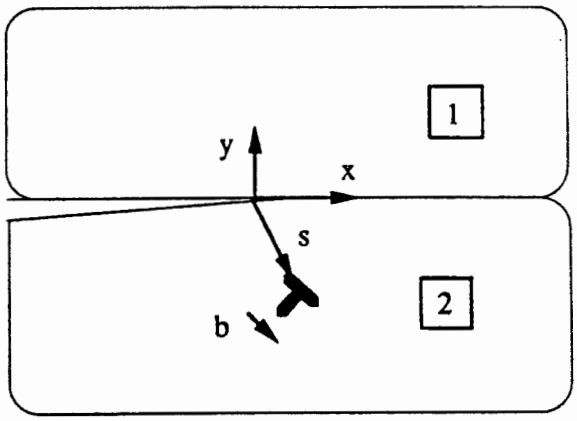

Fig. 4 Interaction of a dislocation with an interface crack tip

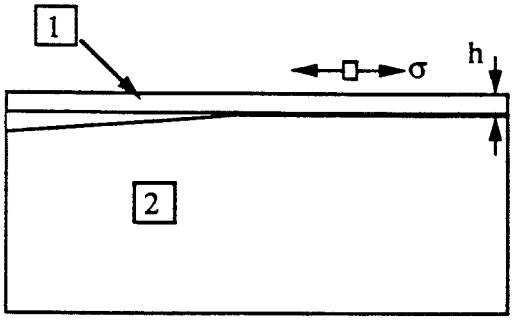

Fig. 5a A thin film on a substrate.

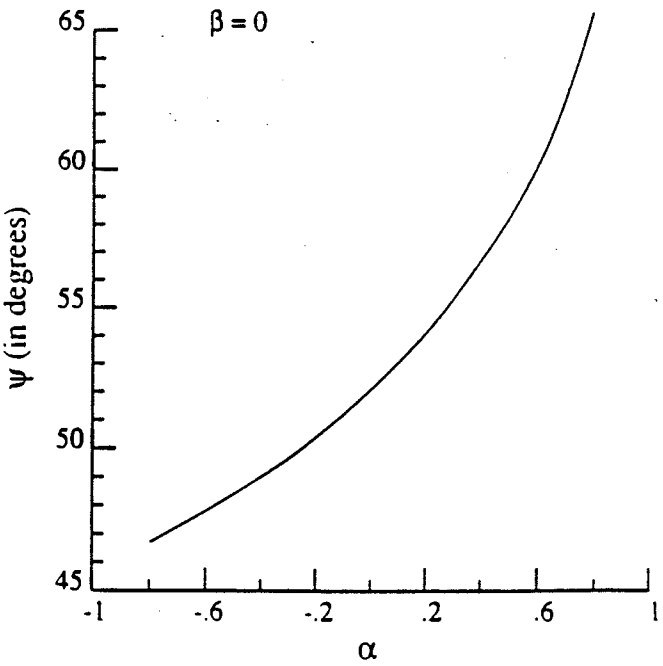

Fig. 5b Phase angle for thin film on substrate

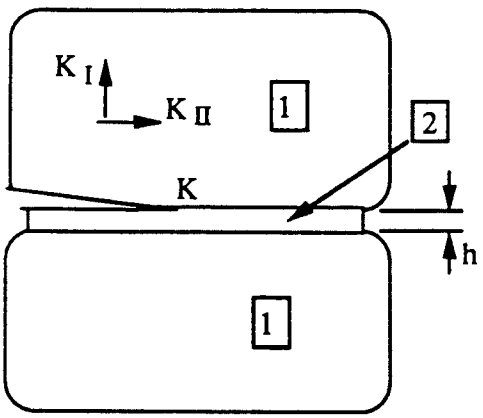

Fig. 6a Sandwich specimens; h is small (when h = 0, KI and KII are the standard stress intensity factors)

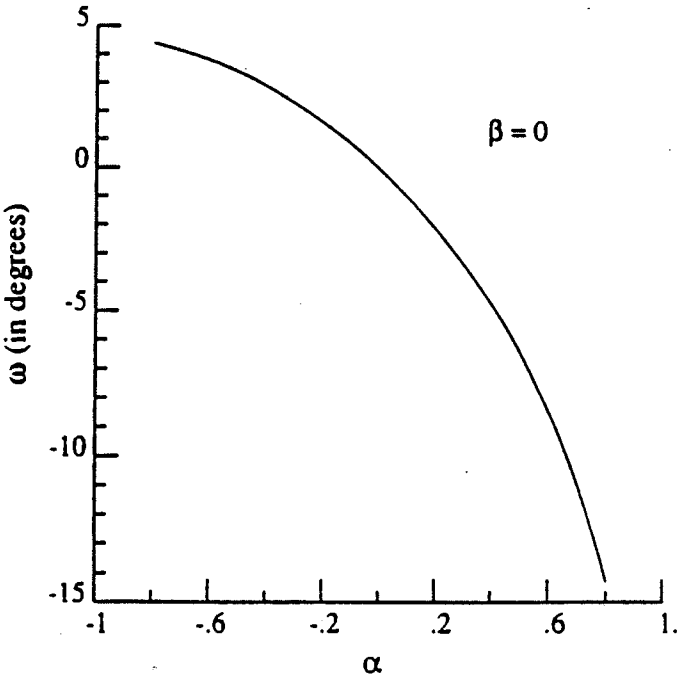

Fig. 6b Phase angle shift for sandwiches

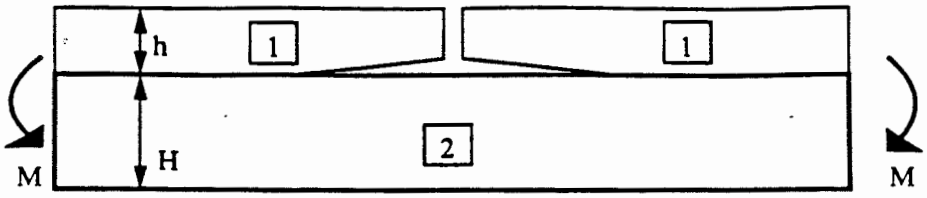

Fig. 7a A bending specimen

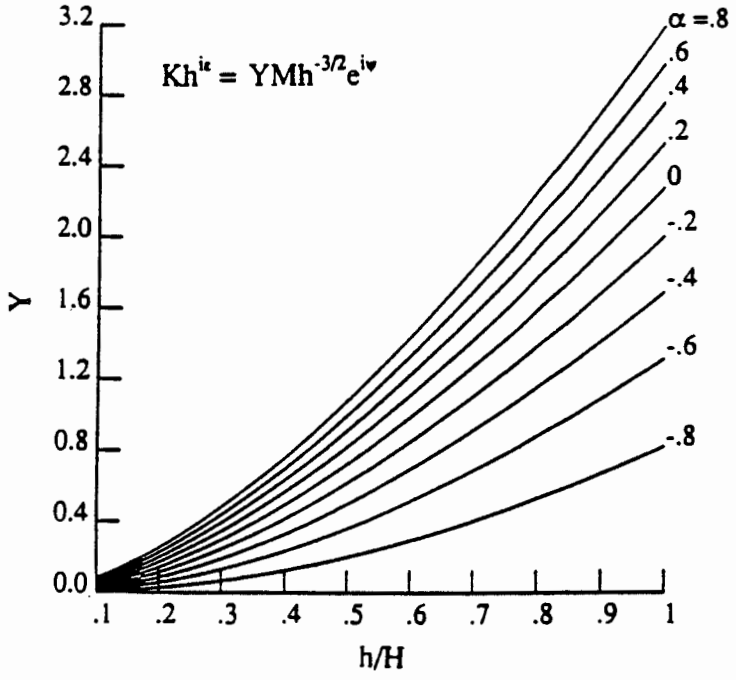

Fig. 7b Pre-factor for stress intensity factor

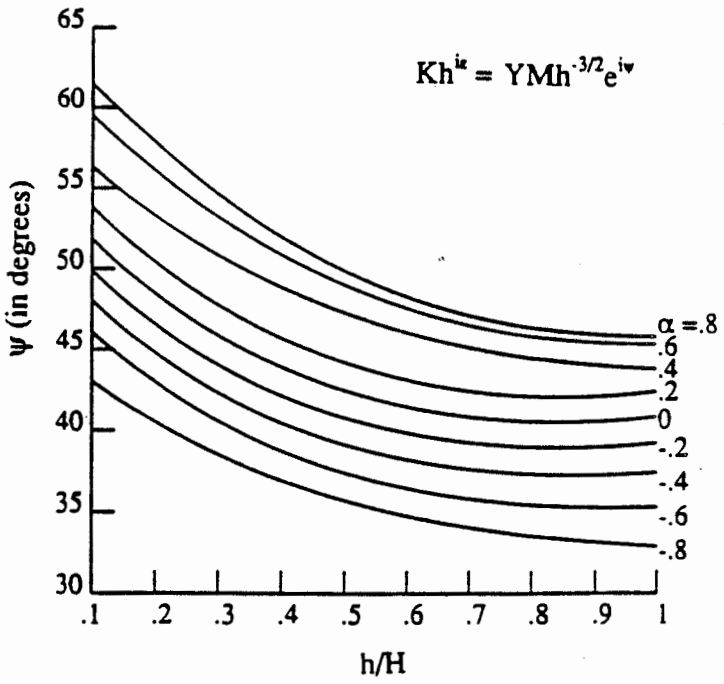

Fig. 7c Phase angle for stress intensity factor

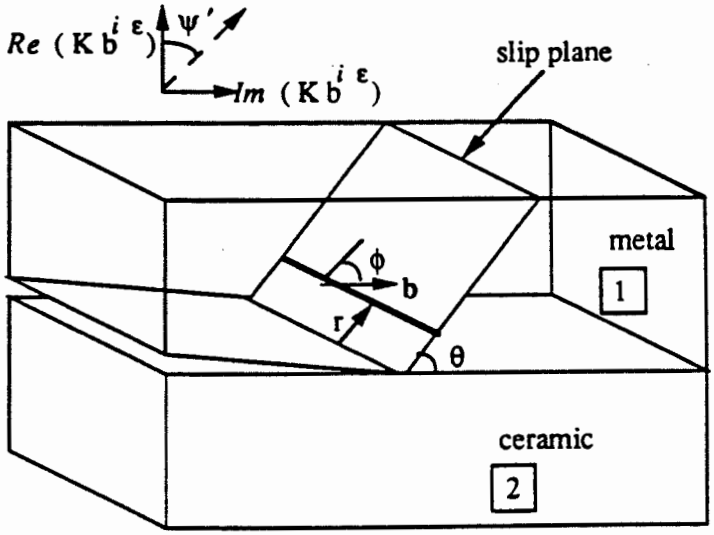

Fig. 8 Dislocation emission from the tip of a metal/ceramic interface crack

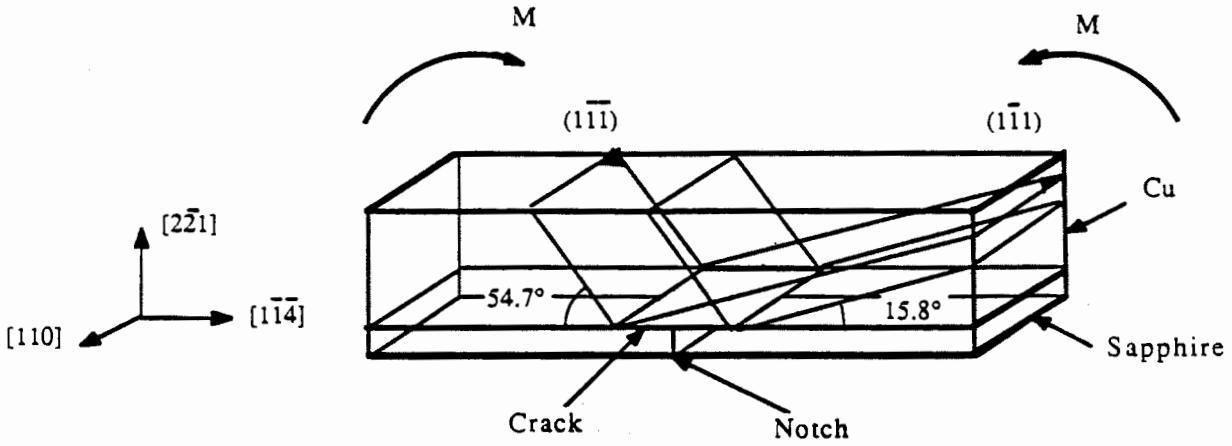

Fig. 9a Cu single crystal with (2$\bar{2}$1) face bonded to sapphire layer; loaded in bending with crack tips along [110]

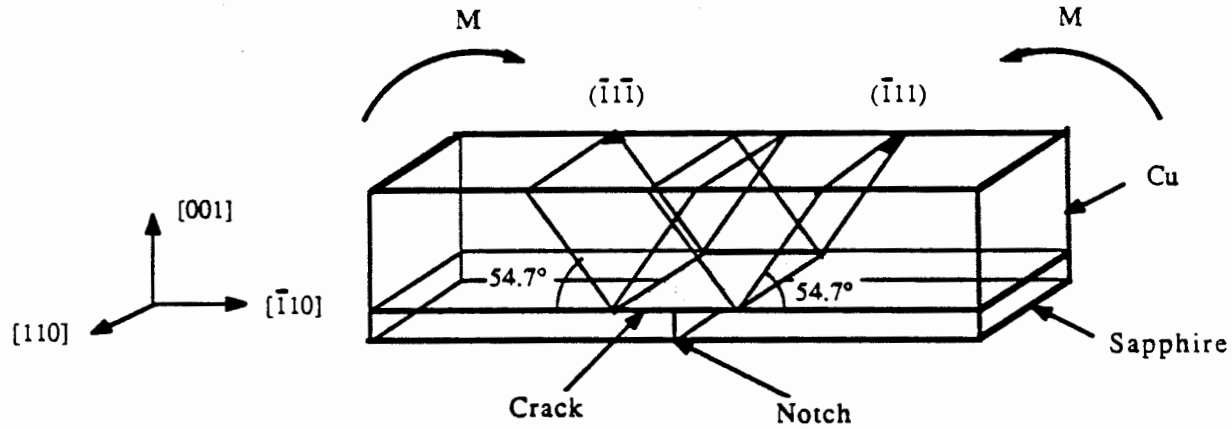

Fig. 9b Cu single crystal with (001) face bonded to sapphire layer; loaded in bending with crack tips along [110]

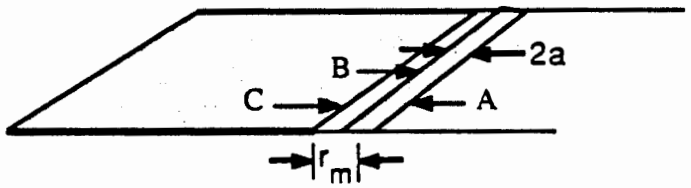

Fig. 9c Microcrack ahead of macrocrack

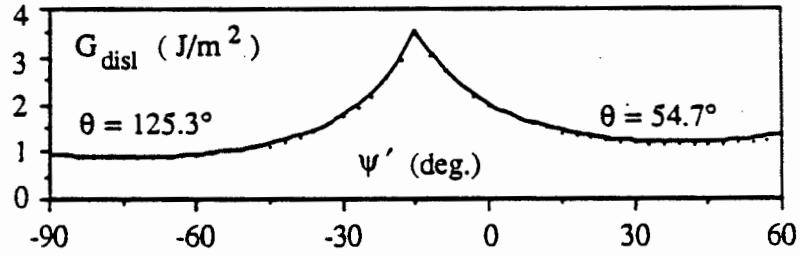

Fig. 10 Dislocation nucleation in Cu; crack tip along [110] ; crack plane is (001)

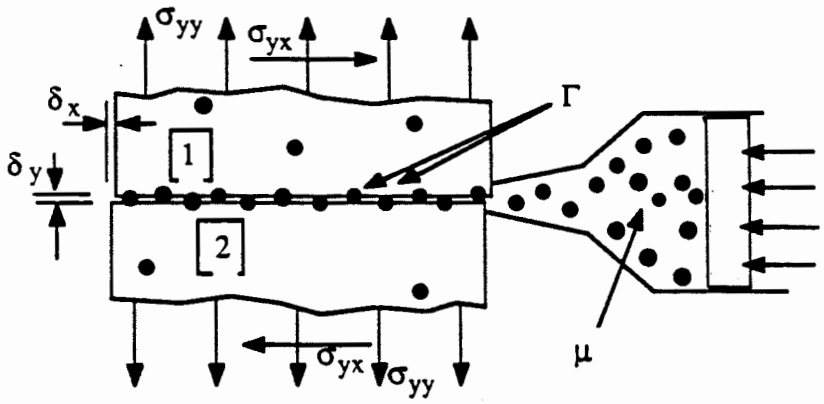

Fig. 11 Dissimilar material interface undergoing decohesion; segregated solutes constrained from composition equilibrium with adjoining bulk phases.

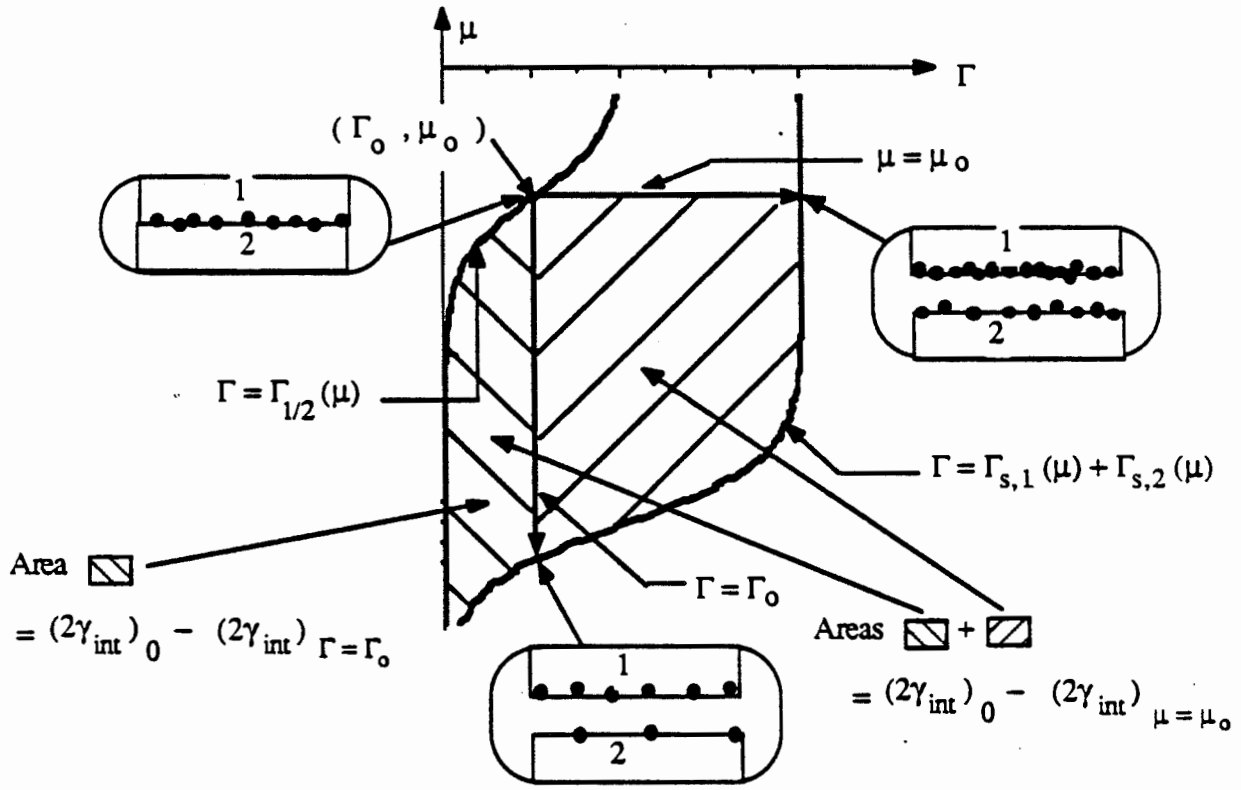

Fig. 12 Use of adsorption isotherms, for unstressed interface and for pair of free surfaces created by separation, to calculate effect of solute adsorption on the ideal work of separation.